Earth and Planetary Science Letters 296 (2010) 210–226

Contents lists available at ScienceDirect

Earth and Planetary Science Letters

journal homepage: www.elsevier.com/locate/epsl

Jurassic–Cretaceous low paleolatitudes from the circum-Black Sea region (Crimea and Pontides) due to True Polar Wander

Maud J.M. Meijers [a,b,*], Cor G. Langereis [a], Douwe J.J. van Hinsbergen [c], Nuretdin Kaymakcı [d], Randell A. Stephenson [e], Demir Altıner [d]

[a] Paleomagnetic Laboratory Fort Hoofddijk, Department of Earth Sciences, Utrecht University, Budapestlaan 17, 3584 CD Utrecht, The Netherlands
[b] Department of Tectonics and Structural Geology, Faculty of Earth and Life Sciences, VU University Amsterdam, De Boelelaan 1085, 1081 HV Amsterdam, The Netherlands
[c] Physics of Geological Processes, University of Oslo, Sem Sælands vei 24, NO-0316, Oslo, Norway
[d] Department of Geological Engineering, Faculty of Engineering, Middle East Technical University, İnönü Bulvarı, 06531-Ankara, Turkey
[e] School of Geosciences, University of Aberdeen, Meston Building, King's College, Aberdeen AB24 3UE, United Kingdom

ARTICLE INFO

Article history:
Received 16 December 2009
Received in revised form 28 April 2010
Accepted 29 April 2010
Available online 11 June 2010

Editor: P.B. DeMenocal

Keywords:
paleomagnetism
Eurasia
Turkey
Ukraine
inclination error
low latitudes
Mesozoic
True Polar Wander

ABSTRACT

In a recent study, paleomagnetic and paleoenvironmental data from Adria (as part of the African plate) suggest a trend toward much lower (~15°) latitudes from Early Jurassic to Earliest Cretaceous at the position of Adria than suggested by the apparent polar wander (APW) paths. The smoothing of existing (APW) paths has most likely caused this low-latitude episode to be overlooked. In this study, we test if the low paleolatitudes in the Jurassic to Early Cretaceous can also be found in Eurasia, i.e. Crimea (Ukraine) and the Pontides (Turkey) that are situated in the present-day Black Sea region. Our Eurasian data suggest the same low Late Jurassic to Early Cretaceous paleolatitudes as shown for Africa. The Jurassic to Lower Cretaceous time span is characterized by Tethys subduction between the African and Eurasian continents and these subduction zones likely functioned as an anchor in the mantle. Therefore, we regard it unlikely that both the African and Eurasian plates moved by >1500 km south and subsequently north with respect to the mantle, as suggested by the paleomagnetic results. True polar wander (TPW) provides a mechanism that rotates the Earth's crust and mantle with respect to its core, and it was recently quantified. The period from 195–135 Ma (Early Jurassic to Earliest Cretaceous) is subject to clockwise TPW, which could well explain our results. We conclude that TPW rather than plate tectonics is the cause of low Late Jurassic to Early Cretaceous African and Eurasian paleolatitudes in the eastern Mediterranean area.

1. Introduction

A recent paleomagnetic study on the Adria terrane, as part of the African continent in the Mesozoic, identified a rapid southward-then-northward movement of Adria within ~50 Myr, from the Early Jurassic to Earliest Cretaceous (Muttoni et al., 2005). These authors suggested that this Middle–Late Jurassic African southward movement, followed by a northward movement is underestimated in the apparent polar wander (APW) path of Besse and Courtillot (2002), as a result of smoothing due to the application of a moving average. In terms of displacement, the Adriatic promontory of Africa would move approximately 1600 km further southward than is expected from the APW path of Besse and Courtillot (2002). The conclusion of Muttoni et al. (2005) was based on new data from Adria and published data from African and North American magmatic rocks that were rotated to northwest African coordinates using the Atlantic plate circuit. The movement towards and away from equatorial latitudes was supported by a corresponding change in latitude suggested by the nature of deep marine sediments in Adria, changing from Lower Jurassic carbonate facies at tropical latitudes to Middle to Upper Jurassic radiolarites at equatorial latitudes, and back again to carbonate facies at tropical latitudes in the Cretaceous. Muttoni et al. (2005) concluded that the underestimated motion of Africa is the result of statistical procedures in the construction of APW paths, and that their revised pole path represents the true motion of the African plate to southerly latitudes in Middle–Late Jurassic times. However, they did not explore the possible reasons for this strong paleolatitudinal shift.

Plate kinematic reconstructions for the period following the break-up of Pangea are based on the constructions of plate circuits from the marine magnetic anomaly record. The placing of the continents with respect to the Earth's magnetic field, which is aligned with the spin axis, is reconstructed using paleomagnetic data. The position of continents with respect to the mantle in the period after 130 Ma is further constrained using hotspot reference frames (Müller et al., 1993; Steinberger and O'Connell, 1998; O'Neill et al., 2005; Torsvik et al.,

* Corresponding author. Paleomagnetic Laboratory Fort Hoofddijk, Department of Earth Sciences, Utrecht University, Budapestlaan 17, 3584 CD Utrecht, The Netherlands.
E-mail address: meijers@geo.uu.nl (M.J.M. Meijers).

0012-821X/$ – see front matter © 2010 Elsevier B.V. All rights reserved.
doi:10.1016/j.epsl.2010.04.052

2008). To filter out or reduce paleomagnetic and geochronologic errors, APW paths are constructed using sliding windows. Consequently, fast motions of the continents are underestimated in APW paths.

However, the movement of a plate recorded in an APW path, is not necessarily entirely unique for that plate, but may share a motion component with all other plates. There are several episodes wherein the entire mantle and crust rotated with respect to the Earth's spin axis. Studies concerning the nature of true polar wander (TPW) have been carried out since the 1950s (Gold, 1955; Goldreich and Toomre, 1969) and periods of TPW and have been reported by Besse and Courtillot (1991; 2002), Evans (Evans, 2003) and Torsvik et al. (Torsvik et al., 2008). TPW results from a redistribution of density inhomogeneities in the mantle, for example caused by the rise of mantle plumes or the subduction of plates (Steinberger and Torsvik, in revision). Since TPW represents a true rotation of the mantle and crust with respect to the Earth's spin axis, it is also recorded in the sedimentary record, through climate controlled facies changes, and flora and fauna variations. Several post-Permian episodes of TPW were recently quantified by Steinberger and Torsvik (2008). One of the proposed intervals of TPW (between 195 and 135 Ma) coincides with the proposed southward movement of Africa of Muttoni et al. (2005). Therefore, there are two possibilities to explain the rapid motion of Africa to southerly latitudes in the Late Jurassic: 1) the African plate moved with respect to the surrounding plates (with major tectonic implications), or 2) all continents moved with respect to the spin axis, and therefore there is no relative motion between the continents other than that expected from plate kinematics. If this rapid motion of Africa is (mainly) caused by TPW, we should find a similar southward motion in the Eurasian plate at longitudes comparable to the Adrian paleolongitude, i.e. with respect to the Euler pole (positioned at the equator) that describes the Jurassic TPW event (Steinberger and Torsvik, 2008). The distance away from this Euler pole determines the paleolatitudinal effect of TPW. Although TPW affects all plates, which means that all plates move together, any differential (tectonically or geodynamically induced) motion is still reflected in the paleomagnetic data. Details on TPW calculation can be found in Steinberger and Torsvik (2008).

In this study, we test if the strong Middle to Late Jurassic southward movement is limited to the African plate, or if the same event can be recognized for the Eurasian plate. To this end, we aimed to determine the paleolatitudinal position of the southern Eurasian margin at the location of the Pontides (Turkey) and Crimea (Ukraine). We have sampled rocks ranging from the Lower Jurassic to Cretaceous. In total, we analyze the results of 27 new sites from the Pontides and Crimea and combine them with our 13 Cretaceous sites from the Pontides (Fig. 1a) (Meijers et al., in press) and with 43 previously published datasets. We corrected, where possible, for the inclination shallowing in sediments with the *E*/*I* method (Tauxe and Kent, 2004).

2. Geological setting

The southern Eurasian margin was affected by the subduction of the Paleo-Tethys and Neo-Tethys oceans since the Paleozoic. The Neo-Tethys opened in the Permian, and sediments attributed to this event are widely distributed in the present-day Mediterranean area (Dercourt et al., 2000; Stampfli and Borel, 2002; Gutierrez-Alonso et al., 2008). The Paleo- and Neo-Tethyan domains were separated by a series of presently east–west distributed "Cimmerian continents" that rifted away from the African margin upon opening of the Neo-Tethys. Following Paleo-Tethys closure, northward subduction of the Neo-Tethys ocean (Fig. 1b) controlled the development of the Eurasian continental margin and led to the formation of several back-arc basins on the overriding plate, of which the Cretaceous–Eocene Black Sea basin is a prominent example. The opening of the Black Sea since Middle to Late Cretaceous times (Okay et al., 1994) accommodated only ~100–150 km (~1–1.5° inclination) of extension (Cloetingh et al., 2003; Starostenko et al., 2004; Shillington et al., 2008), which is well within paleomagnetic errors and an order of magnitude smaller than the African southward movement. Therefore, the opening of the Black Sea is not expected to be significantly reflected in paleomagnetic results from the Pontides. Some authors suggested the presence of a small oceanic basin between the Pontides and Crimea in Triassic to Jurassic times (Küre Ocean) (Şengör and Yilmaz, 1981; Robertson and Dixon, 1984; Stampfli and Borel, 2002; Moix et al., 2008), although the oceanic nature of this basin was challenged by others (Dercourt et al., 2000; Barrier and Vrielynck, 2008).

The Paleozoic and/or older Crimean basement is formed by the thinned margin of the East European Craton (EEC): the Scythian Platform (Fig. 1a) (Stephenson et al., 2004; Saintot et al., 2006b). It is almost entirely covered by Mesozoic–Cenozoic volcano-sedimentary units (Nikishin et al., 2001), that can be subdivided in three units. 1) a lower unit of Triassic to Middle Jurassic (Bathonian) intensely deformed series of turbidites and shales, olistostromes, calc-alkaline volcanics and continental clastics. 2) a middle unit of Upper Jurassic to Lower Cretaceous (Berriasian) platform carbonates that changes eastward into conglomerates and turbidites. The Upper Jurassic platform carbonates are allochtonous thrust slices according to Mileyev et al. (1996), which we regard unlikely, because it would imply that exactly the time interval that is characterized by carbonate deposition is missing in the entire Crimean stratigraphy, except for Kimmeridgian conglomerates and turbidite sequences that can be found in the east of the peninsula. In case the Jurassic carbonates are allochtonous, their displacement would be on the order of tens of kilometers, which is well beyond the resolution of paleomagnetic studies (~2–3°, or ~200–300 km). An episode of folding and thrusting occurred in intra-Berriasian times (~145–140 Ma). 3) an upper unit of Lower Cretaceous (Upper Berriasian) to Eocene rift-related deposits (Zonenshain and Le Pichon, 1986), probably resulting from Black Sea opening (Okay et al., 1994; Banks et al., 1997). The upper unit experienced little deformation, compared to the lower two units (Mileyev et al., 1996; Mileyev et al., 1997; Saintot et al., 1999).

The Pontides constitute the region between the Black Sea in the north and the İzmir–Ankara–Erzincan suture zone in the south, which demarcates the (northern) Neo-Tethyan Ocean in Turkey (Şengör and Yilmaz, 1981). In the studied area, the Pontides consist of two different tectonic blocks: the İstanbul and Sakarya Zones (Fig. 1a) (Okay, 1989). The age of amalgamation of the İstanbul and Sakarya Zones has been a matter of debate, and proposed ages range from Early Jurassic (Şengör et al., 1980) to early Late Cretaceous (Tüysüz, 1999). In the latter case, it was thought to result from closure of the so-called "Intra-Pontide ocean", a narrow (~300 km) oceanic basin (Okay et al., 1994; Robertson and Üstaömer, 2004). Recent studies by Bozkurt et al. (2008) and Okay et al. (2008) revealed, however, that the İstanbul and Sakarya Zones amalgamated with Eurasia during the Paleozoic, with possibly some post-Triassic reactivation (Okay et al., 2008).

The Sakarya Zone constitutes an intensely deformed Variscan (i.e. Eurasian) basement and the locally metamorphosed pre-Jurassic Karakaya Complex (Tekeli, 1981; Okay et al., 1991). The İstanbul Zone comprises a non-metamorphic Ordovician to Carboniferous sedimentary sequence that experienced mild deformation during the Permo-Carboniferous, overlain by Triassic sediments. Its stratigraphy is generally correlated to the Moesian Platform, from which it separated during western Black Sea opening in the Early Cretaceous (Görür, 1988; Okay et al., 1994).

The Lower Jurassic of the Sakarya Zone consists of shallow marine clastics, and includes some ammonitico-rosso levels (Altıner et al., 1991). In the eastern part of the Sakarya Zone, the Lower to Middle Jurassic sequences include volcanics and volcanoclastics (Yılmaz et al., 2003; Yılmaz and Kandemir, 2006). The Upper Jurassic to Lower Cretaceous deposits in the entire Pontides consist of platform carbonates. Carbonate deposition in the Sakarya Zone commenced slightly earlier than in the İstanbul Zone, namely in the Middle Jurassic (Callovian). Similar to Crimea, the Lower Cretaceous (Hauterivian) to

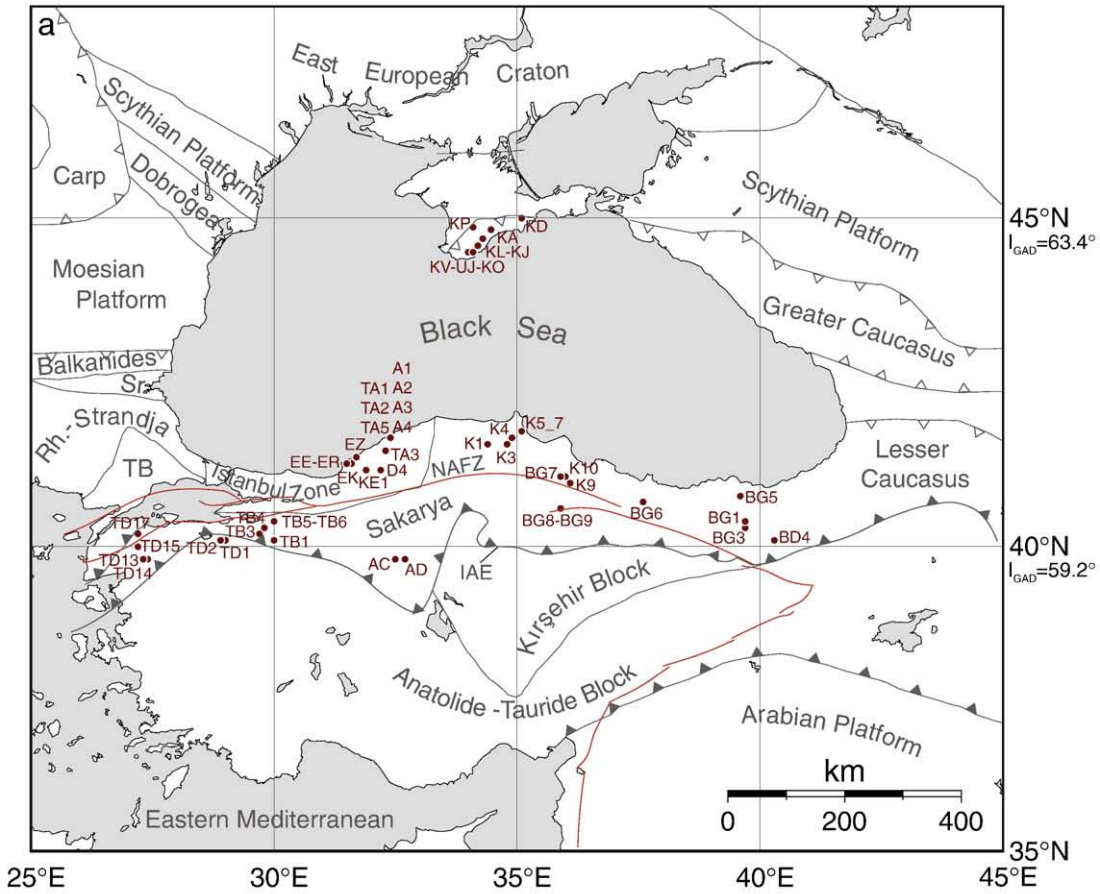
a
East European Craton
Scythian Platform
Carp
Dobrogea
Moesian Platform
Black Sea
Scythian Platform
Greater Caucasus
Balkanides
Sr
Rh.-Strandja
TB
Istanbul Zone
NAFZ
Sakarya
Lesser Caucasus
IAE
Kırşehir Block
Anatolide -Tauride Block
Arabian Platform
Eastern Mediterranean
km
0 200 400
45°N
I_GAD=63.4°
40°N
I_GAD=59.2°
35°N
25°E 30°E 35°E 40°E 45°E
KP KA KD KL-KJ KV-UJ-KO
A1 TA1 A2 TA2 A3 TA5 A4 EZ TA3 EE-ER EK KE1 D4
K4 K5_7 K1 K3 BG7 K10 K9
BG5 BG6 BG8-BG9 BG1 BG3 BD4
TD17 TB4 TB3 TB5-TB6 TB1 TD15 TD2 TD1 TD13 TD14
AC AD

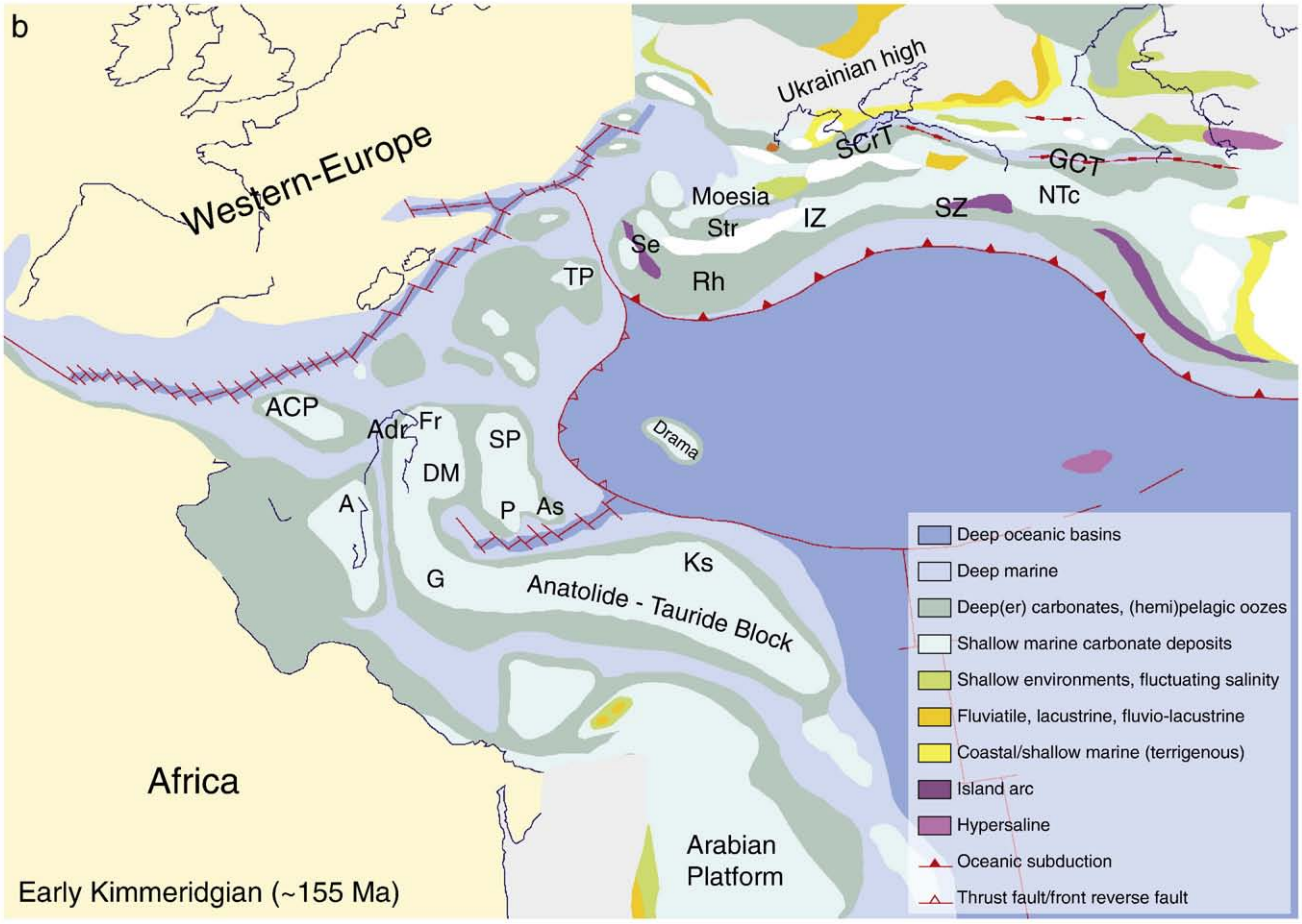
b
Western-Europe
Ukrainian high
SCrT
GCT
NTc
Moesia Str
IZ
SZ
Se
Rh
TP
ACP
Adr
Fr
SP
DM
A
P
As
Drama
G
Ks
Anatolide - Tauride Block
Africa
Arabian Platform
Early Kimmeridgian (~155 Ma)
Deep oceanic basins
Deep marine
Deep(er) carbonates, (hemi)pelagic oozes
Shallow marine carbonate deposits
Shallow environments, fluctuating salinity
Fluviatile, lacustrine, fluvio-lacustrine
Coastal/shallow marine (terrigenous)
Island arc
Hypersaline
Oceanic subduction
Thrust fault/front reverse fault

Eocene rift-related deposits are related to opening of the Black Sea (Görür, 1997).

It is of importance here that Africa and Eurasia were separated in the Jurassic by a Tethyan subduction zone (Ricou et al., 1998; Dercourt et al., 2000; Stampfli and Borel, 2004; van Hinsbergen et al., 2005; Barrier and Vrielynck, 2008; Schmid et al., 2008). Evidence for subduction in the studied area is however a matter of debate. In the Pontides, Crimea and the Greater Caucasus (Fig. 1a), Early and Middle Jurassic rift basin development probably took place in a back-arc setting, driven by the northward subduction of the Neo-Tethys south of the Pontides. This is evidenced by the large amount of volcanogenic sediments in Crimea and the eastern Pontides, and the dominantly volcanic Bathonian–Bajocian interval in the Greater Caucasus (Robinson et al., 1995; Banks and Robinson, 1997; Nikishin et al., 2001; Saintot et al., 2006a; Saintot et al., 2006b). The subduction zones in the Jurassic Tethyan realm acted as an anchor in the mantle, and therefore relatively fast motion of both the African and Eurasian continents with respect to the mantle is unlikely.

3. True Polar Wander

True Polar Wander (TPW) events were quantified in several studies for the last 200 Myr (Besse and Courtillot, 1991; Prevot et al., 2000; Besse and Courtillot, 2002). Recently, Steinberger and Torsvik (2008) calculated TPW over the last 320 Myr, by assessing the APW paths of all continents. For periods younger than 130 Ma, the paths were compared to a moving hotspot reference frame. By definition, a TPW event has an equatorial Euler pole. The paleomagnetic expression of TPW is dependent on the position of the sampling site with respect to the Euler pole during TPW, because it determines the sense of motion a location would experience during TPW.

Four intervals of TPW were identified by Steinberger and Torsvik (2008). In the period from 250–220 Ma a counterclockwise TPW (18°) around an equatorial Euler pole at 15°W would cause large northward movements in the present-day circum-Black Sea region, located at the southern margin of Eurasia. The effect of TPW was compensated in the period of 195–145 Ma with a clockwise movement around the same Euler pole. This was followed by dominantly east–west movements from 145–135 Ma, caused by 10° clockwise rotation around an equatorial Euler pole located at 37.5°E, compensated by a next period of counterclockwise TPW from 110–100 Ma that would have resulted in northwestward movement of the circum-Black Sea area. Therefore, in the case that TPW, instead of tectonics, has been the (main) mechanism to transport Adria to low latitudes, the present-day circum-Black Sea region should have experienced a similar, and even more pronounced movement.

4. Paleomagnetic sampling, analysis and reliability criteria

4.1. Paleomagnetic sampling and analysis

Sampled lithologies vary from limestones to sandstones, siltstones, shales, marls, clays, calcarenites and volcanoclastics (see Table 1 and Supplementary data). Cores were collected using a motor drill. Sample orientations were measured with a magnetic compass and corrected for the present-day declination. In most cases, cores were long enough to provide multiple specimens from a single core. Therefore, the number of demagnetized specimens is sometimes higher than the number of sampled cores (Table 1). For absolute ages, we correlate biostratigraphic ages to the GTS2004 timescale (Ogg, 2004; Ogg et al., 2004). For several sampled sites, new biostratigraphic ages from limestones were determined by D. Altıner. Ages for all sites can be found in the Supplementary data in Appendix A and in Table 1.

Magnetic carriers were determined by performing thermomagnetic runs and isothermal remanent magnetization (IRM) curves. IRM acquisition curves were performed on samples that had been heated already until 150 °C and used for AF demagnetization (Fig. 2a–f). Before IRM acquisition curves determination, all specimens were first demagnetized until 300 mT in three orthogonal directions, to minimize the influence of magnetic interaction and thermal activation (Heslop et al., 2004). The IRM was acquired in 57 steps until 700 mT, with an in-home developed robot assisted and fully automated 2G DC SQUID cryogenic magnetometer (noise level 10^{-12} A m^2). The IRM measurements were analyzed using the cumulative log-Gaussian approach to identify the different coercivity components with the method developed by Kruiver et al. (2001). The diagrams were interpreted with either two or three magnetic components, overlapping in coercivity spectrum, to provide a best-fit to the IRM curves. The low intensity and low coercivity component that is usually observed using this method results from a skewed data distribution and has no physical meaning (Heslop et al., 2004). The magnetic components can be characterized by the saturation isothermal remnant magnetization (SIRM), the peak field, at which half of the SIRM is reached ($B_{1/2}$) and the dispersion of its corresponding cumulative log-normal distribution (DP) (Kruiver et al., 2001). The thermomagnetic runs were carried out in air, using a modified horizontal translation type Curie balance, with a sensitivity of $\sim 5\times10^{-9}$ Am^2 (Mullender et al., 1993) (Fig. 2g–i). Approximately 40 mg of powdered rock samples were put into a quartz glass sample holder and were held in place by quartz wool. Heating and cooling rates were 10 °C/min. Temperatures were increased to a maximum of 700 °C.

Samples were demagnetized using thermal and alternating field (AF) demagnetization methods, or a combination of both methods. Thermal demagnetization was carried out in a magnetically shielded oven, with steps of 30 °C–50 °C up to a maximum of 540 °C. AF demagnetization up to a maximum of 90 mT was carried out with steps of 3–20 mT. A 2G Enterprises horizontal 2G DC SQUID cryogenic magnetometer with a noise level of 3×10^{-12} A m^2 was used to measure the natural remanent magnetization (NRM) of all samples. The AF demagnetization procedure and measurement of the samples was performed with an in-home developed robot assisted and fully automated 2G DC SQUID cryogenic magnetometer.

Test sets of samples were demagnetized both thermally and by alternating field, to allow comparison of both applied techniques (e.g. Gong et al. (2008)). To remove possible stress in magnetite grains caused by surface oxidation at low temperatures (Van Velzen and Zijderveld, 1995), most AF demagnetized samples were heated to 150 °C before demagnetization (see procedures in Gong et al. (2008)). Several samples of site UJ that were AF demagnetized were heated until 210 °C before AF demagnetization, while part of the samples of site TD14 were heated until 300 °C before demagnetization, the temperatures at which a secondary component was generally removed.

Demagnetization diagrams of the natural remanent magnetization (NRM) were plotted as orthogonal vector diagrams (Zijderveld, 1967) (Fig. 3). Results from generally five to eight successive temperature or AF steps were analyzed by principal component analysis (Kirschvink, 1980) to determine the characteristic remanent magnetization (ChRM) in the samples (Table 1).

Fisher statistics (Fisher, 1953) were used to calculate directional and virtual geomagnetic pole (VGP) means (Fig. 4). Because secular

Fig. 1. a) Map of the circum-Black Sea area indicating the sampled sites, the Izmir–Ankara–Erzincan suture (IAE), the North Anatolian Fault Zone (NAFZ), and the regional structural framework. TB = Thrace Basin; Rh.-Strandja = Rhodope–Strandja Massif; Carp = Carpathians. b) Early Kimmeridgian paleogeographic reconstruction after Dercourt et al. (2000), indicating the position of the main tectonic blocks in the western Tethyan realm, and their proposed position with respect to the plate boundaries. A = Apulia; ACP = Appennine Carbonate Platform; Adr = Adria; As = Asteroussia; DM = Dalmatia; Fr = Friuli; G = Gavrovo; GCT = Greater Caucasus Through; IZ = Istanbul Zone; Ks = Kırşehir Massif; NTc = Northern Transcaucasus; P = Parnassos; Rh = Rhodopes; SCrT = South Crimean Through; Se = Severin; SP = Serbo = Pelagonian; Str = Strandja; SZ = Sakarya Zone; TP = Tisza Plate. Adria is part of the African plate, whereas the Pontides and Crimea are part of the Eurasian plate. Note that we correlated the Early Kimmeridgian to the GTS2004 timescale (Ogg, 2004).

Table 1
Table showing all data from our study. Upper table: Site number **bold**: accepted site. Rej. = rejection criterium (see Section 4.2); Site lat. = site latitude; Site long. = site longitude; Age = age assigned according to Ogg (2004) and Ogg et al. (2004); Δ Age = age error; Ns/Nm = number of sampled cores/number of measured specimens; Ni/NvD = number of interpreted directions/number of directions that are remaining after applying a variable cut-off (Vandamme, 1994); D = declination; ΔD_x = declination error; I = inclination; ΔI_x = inclination error; k = estimate of the precision parameter determined from the ChRM directions; α_{95} = cone of confidence determined from the ChRM directions. All values are given before and after correction for bedding tilt. λ = pole latitude; ϕ = pole longitude; K = precision parameter determined from the mean virtual geomagnetic pole (VGP) direction; A_{95} = cone of confidence determined from the mean VGP direction. Lower table: The inclination after correction for inclination (I) error results from 5000 bootstraps of TK03.GAD, with 95% lower and upper bounds (I_l, I_u), while I_{EI} is the inclination resulting from intersection of the distribution with TK03.GAD (Tauxe and Kent, 2004). λ is the corresponding corrected latitude, with 95% lower and upper bounds (λ_l, λ_u), ΔD_x, ΔI_x, K and A_{95} are as mentioned above for the unflattened datasets. * Site TD13 was rejected for reasons discussed in the text.

			ChRM directions-in situ											
Site	Rej.	Rock type	Site lat.	Site long.	Age	Δ Age	Ns/Nm	Ni/NvD	D	ΔD_x	I	ΔI_x	k	α_{95}
Crimea														
KV		**Limestone**	**44.5**	**34.0**	**142.8**	**2.7**	**42/44**	**29/28**	**355.4**	**7.2**	**52.7**	**6.3**	**30.5**	**5.0**
KO		**Limestone**	**44.5**	**34.1**	**153.3**	**7.8**	**78/107**	**107/105**	**346.2**	**1.5**	**54.2**	**1.2**	**184.4**	**1.0**
UJ		**Limestone**	**44.5**	**34.1**	**153.3**	**2.5**	**101/129**	**124/115**	**352.2**	**1.4**	**19.7**	**2.5**	**53.7**	**1.8**
KP		**Clays**	**44.9**	**34.1**	**112.3**	**12.7**	**128/113**	**84/79**	**2.9**	**3.0**	**52.2**	**2.7**	**46.8**	**2.4**
KL	3, 5, 6, 7	Siltstones	44.6	34.2	169.7	2.0	17/08	08/07	108.2	8.4	1.3	16.9	19.0	13.0
KJ	5, 6, 7	Sandstones	44.6	34.2	169.7	2.0	33/25	24/19	51.6	9.1	43.3	10.6	20.3	7.6
KA		**Limestone**	**44.7**	**34.3**	**148.1**	**2.7**	**118/147**	**91/82**	**30.5**	**4.9**	**61.7**	**3.0**	**35.9**	**2.6**
KH	3	Calcarenites and clays	44.8	35.1	163.0	1.8	97/36	0/0						
KD	7	Calcareous silt/ sandstones and clayey marls	45.0	35.1	135.1	5.1	87/87	119/110	0.3	7.8	74.7	2.2	38.0	2.2
KF	3	Calcarenites and clays	45.0	35.4	148.2	2.7	97/14	0/0						
Pontides														
TD17	6	Red carbonates	40.2	27.2	63.2	7.4	15/14	10/10	312.7	10.5	59.9	7.0	66.9	6.0
TD15	2?, 3	Calcarenites and siltstones	40.0	27.2	186.3	3.3	10/17	12/12	353.7	5.5	55.4	4.3	124.3	3.9
TD14		**Limestones**	**39.8**	**27.4**	**160.2**	**4.5**	**59/108**	**95/92**	**155.2**	**1.6**	**−21.4**	**2.9**	**50.7**	**2.1**
TD13		Limestones	39.8	27.4	112.3	12.7	70/83	80/70	308.5	2.7	30.3	4.2	40.6	2.7
TD2		**Limestones**	**40.1**	**28.9**	**160.2**	**4.5**	**36/46**	**29/29**	**333.0**	**8.6**	**64.5**	**4.6**	**41.6**	**4.2**
TD1	2?, 6	Sandstones	40.1	29.0	186.3	3.3	12/12	11/11	350.2	6.5	55.8	5.1	119.5	4.2
TB3	3, 5, 6	Pink limestones	40.2	29.7	163.0	1.8	103/29	21/21	111.0	6.8	−18.7	12.4	11.1	10.0
TB4	2?, 3, 4, 6	Limestones	40.3	29.8	130.4	30.8	15/15	13/13	11.7	15.3	59.3	10.4	22.7	8.9
TB5	5, 6	Red limestones	40.4	30.0	186.3	3.3	73/27	20/23	330.6	5.0	−3.0	10.0	24.4	6.7
TB6	6	Siltstones	40.4	30.0	186.3	3.3	26/10	10/10	312.5	5.8	−13.5	11.0	36.9	8.1
TB1	3	Limestones	40.1	30.0	163.0	1.8	15/13	0/0						
TA3	2?, 3, 4, 5, 6	Limestones	41.5	32.3	130.4	30.8	15/9	8/8	14.6	30.6	60.7	19.2	13.4	15.7
TA1	3, 4, 5, 6	Limestones	41.7	32.4	130.4	30.8	24/15	10/10	35.8	99.9	61.6	83.9	1.0	99.9
AC	5, 6	Limestones	39.8	32.5	144.5	2.5	43/20	19/19	272.6	17.6	62.7	10.2	15.0	9.0
AD	3	Limestones	39.8	32.7	142.5	12.5	60/30	0/0						
BG8	5, 6	Limestones/dolomites	40.6	35.9	163.0	1.8	56/10	8/8	318.7	7.9	39.4	10.2	56.4	7.4
BG9	5, 6	Grainstones	40.6	35.9	150.6	14.1	62/15	14/11	173.0	11.1	−41.3	13.7	25.7	9.2
BG3	2?, 5, 6	Red siltstones	40.3	39.7	187.6	12.0	82/16	11/11	9.0	19.0	67.5	8.6	31.7	8.2
Pontides–previous study–Meijers et al. (in press)														
ER	5,6	Clays/volcanoclastics	41.3	31.5	86.4	2.9	16/14	14/14	331.5	8.2	40.3	10.3	24.2	8.3
EE	6	Red pelagic limestones	41.3	31.5	86.4	2.9	15/13	13/12	169.2	6.4	−44.6	7.3	56.7	5.8
EK	6	Red pelagic limestones	41.3	31.6	86.4	2.9	19/14	14/14	328.6	3.2	36.6	4.4	141.0	3.4
A4	6	Red pelagic limestones	41.7	32.4	86.4	2.9	10/7	7/7	210.5	9.9	−44.2	11.3	28.5	11.5
A1	5, 6	Shales	41.7	32.4	121.0	9.0	14/14	14/14	21.3	12.3	19.2	22.2	9.9	13.3
A3	5, 6	Shales	41.7	32.4	121.0	9.0	14/14	7/7	45.1	11.5	31.9	17.3	27.9	11.6
TA2		**Red pelagic limestones**	**41.7**	**32.4**	**86.4**	**2.9**	**149/124**	**89/86**	**336.5**	**2.4**	**42.2**	**2.9**	**47.2**	**2.3**
TA5		**Volcanoclastics**	**41.7**	**32.4**	**84.7**	**1.2**	**68/121**	**117/115**	**186.4**	**1.9**	**−46.1**	**2.1**	**64.5**	**1.7**
K3	4, 5, 6	Shales	41.6	34.8	114.8	15.2	12/14	14/13	188.0	17.3	44.0	19.7	7.1	16.7
K5_7	5,6	Limestones/marls	41.8	35.1	74.5	9.0	19/21	11/11	212.9	11.1	−16.6	20.7	11.4	14.1
BG7	6	Red pelagic limestones	41.1	35.9	86.4	2.9	43/27	17/17	85.3	4.2	35.4	6.0	78.9	4.0
K10	6	Red pelagic limestones	41.1	36.0	86.4	2.9	7/13	13/13	77.0	2.2	37.4	3.0	324.6	2.3
K9	5, 6	Red pelagic limestones	41.0	36.1	86.4	2.9	13/14	14/9	31.3	2.9	6.0	5.7	326.0	4.6

TK03 corrected datasets

			No cut-off											
Site	Age	Δ Age	D	I	I_{EI}	I_l	I	I_u	λ_l	λ	λ_u	K	A_{95}	ΔD_x	ΔI_x
KO	153.3	7.8	332.0	30.2	32.4	30.3	32.0	41.0	16.3	**17.4**	23.5	385.4	0.7	0.7	1.1
UJ	153.3	2.5	342.8	32.7		31.2	33.8	36.4	16.8	**18.5**	20.2	27.2	2.5	2.6	3.8
KP	112.3	12.7	351.5	58.6	64.2	58.2	61.2	78.3	38.9	**42.3**	67.5	24.9	3.2	4.2	2.8
KA	148.1	2.7	335.1	51.1		50.9	53.8	71.6	31.6	**34.3**	56.4	13.0	4.3	5.2	4.2
TD14	160.2	4.5	166.6	−29.8	−39.5	−31.0	−38.5	−50.2	16.7	**21.7**	31.0	47.0	2.1	2.3	2.7
TA2	86.4	2.9	324.4	49.2	54.8	49.8	55.0	68.7	30.6	**35.5**	52.1	40.5	2.4	3.0	2.2
TA5	84.7	1.2	170.1	−44.0	−48.5	−44.2	−46.3	−65.2	25.9	**27.6**	47.3	92.6	1.4	1.6	1.6

variation of the Earth's magnetic field induces scatter in paleomagnetic directions, which is near-Fisherian at the poles, but gradually becomes more ellipsoidal towards the equator (Creer et al., 1959; Tauxe and Kent, 2004), we calculated the VGPs from all directions. Subsequently, a variable cut-off (Vandamme, 1994) was applied to remove outliers from the datasets (e.g. from excursions,

ChRM directions-tilt corrected								VGPs-tilt corrected			
Ni/NvD	D	ΔD_x	I	ΔI_x	Paleolatitude	k	α_{95}	λ	φ	K	A_{95}
29/28	**344.0**	**4.7**	**27.0**	**7.7**	**14.3**	**30.5**	**5.0**	**56.9**	**−116.8**	**36.7**	**4.6**
107/105	**332.0**	**0.7**	**30.3**	**1.0**	**16.3**	**305.2**	**0.8**	**53.2**	**−97.1**	**470.7**	**0.6**
124/115	**342.7**	**1.6**	**33.8**	**2.3**	**18.5**	**53.7**	**1.8**	**60.3**	**−111.3**	**76.5**	**1.5**
84/81	**353.6**	**3.8**	**58.6**	**2.6**	**39.3**	**44.2**	**2.4**	**82.7**	**−103.3**	**30.3**	**2.9**
08/07	110.5	10.9	28.0	17.6	14.9	19.0	13.0	−3.5	99.3	28.5	10.6
24/22	19.8	10.5	49.1	10.4	30.0	15.6	8.1	68.6	160.6	12.6	9.1
91/82	**331.3**	**3.3**	**50.9**	**3.1**	**31.6**	**36.8**	**2.6**	**64.1**	**−76.2**	**31.1**	**2.8**
0/0											
119/113	350.9	2.3	33.8	3.4	18.5	28.5	2.5	62.4	−126.0	36.9	2.2
0/0											
10/10	2.2	6.5	39.8	8.2	22.6	66.8	6.0	72.3	−159.5	66.9	6.0
12/12	346.7	4.1	42.7	4.8	24.8	124.0	3.9	71.1	−112.6	139.0	3.7
95/92	**166.1**	**1.8**	**−29.9**	**2.9**	**16.0**	**48.9**	**2.1**	**−63.3**	**58.4**	**70.5**	**1.8**
80/75	305.5	5.1	64.8	2.7	46.7	43.3	2.5	50.5	−34.0	23.0	3.5
29/29	**24.5**	**4.8**	**44.9**	**5.3**	**26.4**	**41.5**	**4.2**	**65.5**	**145.2**	**40.5**	**4.3**
11/11	13.0	4.2	29.7	6.5	15.9	119.7	4.2	63.3	−179.8	131.6	4.0
21/21	85.3	17.4	58.3	12.3	39.0	11.1	10.0	27.1	90.1	6.5	13.5
12/10	78.3	8.9	64.7	4.7	46.6	121.4	4.4	35.2	85.2	63.1	6.1
23/23	250.2	9.1	−35.0	13.0	19.3	11.0	9.5	−27.2	−62.9	13.4	8.6
10/10	299.8	6.9	−30.5	10.7	16.4	36.9	8.1	10.4	−92.2	54.0	6.6
0/0											
8/8	324.6	99.9	78.9	14.9	68.8	12.4	15.7	57.1	9.4	5.2	26.8
10/10	329.4	99.9	61.3	84.6	42.4	1.0	99.9	67.4	−45.5	1.0	99.9
19/18	315.7	8.9	35.9	12.4	19.9	18.5	8.3	47.3	−72.0	18.1	8.4
0/0											
8/8	13.0	19.1	63.9	10.4	45.6	33.8	9.7	79.3	93.9	18.5	13.2
14/11	175.8	12.3	−46.6	13.1	27.9	25.7	9.2	−76.8	52.4	18.7	10.8
11/11	18.3	40.1	71.4	13.8	56.0	11.7	13.9	70.2	70.9	5.6	21.1
14/14	320.2	9.0	48.2	9.1	29.2	24.1	8.3	55.7	−66.2	26.7	7.8
13/12	170.0	5.9	−39.7	7.5	22.5	56.7	5.8	−69.5	58.7	65.1	5.4
14/14	322.6	3.9	47.9	4.0	29.0	138.1	3.4	57.3	−68.5	136.9	3.4
7/7	213.3	9.7	−41.5	11.9	15.0	10.4	12.9	−57.1	−35.3	47.2	8.9
14/14	18.9	12.2	28.1	19.6	15.0	10.4	12.9	58.7	175.4	12.4	11.8
7/7	33.1	18.7	53.6	15.9	34.1	27.9	11.6	63.0	127.7	16.3	15.4
89/86	**325.3**	**2.6**	**48.8**	**2.6**	**29.7**	**53.4**	**2.1**	**59.7**	**−69.6**	**47.0**	**2.3**
117/115	**169.6**	**1.4**	**−43.9**	**1.6**	**25.7**	**112.1**	**1.2**	**−71.8**	**63.9**	**113.6**	**1.2**
14/12	186.2	14.9	−43.6	17.2	25.5	12.2	12.9	−73.1	15.2	11.4	13.4
11/11	208.3	7.7	−30.2	12.0	16.2	41.5	7.2	−54.7	−16.9	39.2	7.4
17/17	74.7	4.1	43.1	4.8	25.1	114.2	3.4	27.3	115.4	95.1	3.7
13/13	55.9	2.7	43.0	3.2	25.0	324.4	2.3	41.4	127.2	284.4	2.5
14/11	36.8	11.8	42.9	13.9	24.9	12.1	13.7	55.5	142.4	19.3	10.7

TK03 after Vandamme cut-off												
D	I	I_{EI}	I_l	I	I_u	λ_l	λ	λ_u	K	A_{95}	ΔD_x	ΔI_x
332.0	30.3		30.0	30.9	35.9	16.1	**16.7**	19.9	454.2	0.6	0.7	1.0
342.7	33.8		32.8	35.4	41.1	17.9	**19.6**	23.6	75.1	1.5	1.6	2.3
353.6	58.6		57.9	60.1	71.6	38.6	**41.0**	56.4	30.4	2.9	3.8	2.6
331.3	50.9		49.8	52.1	59.6	30.6	**32.7**	40.4	31.1	2.8	3.4	3.1
166.1	−29.9	−32.7	−29.1	−32.0	−39.4	15.6	**17.4**	22.3	65.9	1.8	1.9	2.8
325.3	48.8	49.9	48.2	50.6	59.4	29.2	**31.3**	40.2	46.8	2.3	2.7	2.4
169.6	−43.9	−43.9	−43.6	−45.0	−54.5	25.5	**26.6**	35.0	112.0	1.2	1.4	1.5

reversal transitions or other outliers) and the errors in declination (ΔD_x) and inclination (ΔI_x) were calculated following Butler (1992) (Table 1).

Since we sampled sedimentary rocks, we corrected sufficiently large datasets for a possible shallowing of inclination in sediments caused by compaction during burial with the elongation/inclination (E/I) method

a

KV3.1A

component	contribution	SIRM	log($B_{1/2}$)	$B_{1/2}$	DP
	%	A/m	mT	mT	mT
1	86.8	2.26E+07	1.66	45.7	0.30
2	11.5	3.00E+06	3.00	1000.0	0.26
3	1.7	4.50E+05	1.12	13.2	0.12

b

TD14.20A

component	contribution	SIRM	log($B_{1/2}$)	$B_{1/2}$	DP
	%	A/m	mT	mT	mT
1	84.8	4.62E+07	1.75	56.2	0.31
2	13.8	7.50E+06	2.75	562.3	0.37
3	1.5	8.00E+05	1.00	10.0	0.20

c

KO1.25B

component	contribution	SIRM	log($B_{1/2}$)	$B_{1/2}$	DP
	%	A/m	mT	mT	mT
1	95.2	1.77E+08	1.65	44.7	0.26
2	2.2	4.00E+06	2.44	275.4	0.25
3	2.7	5.00E+06	1.00	10.0	0.20

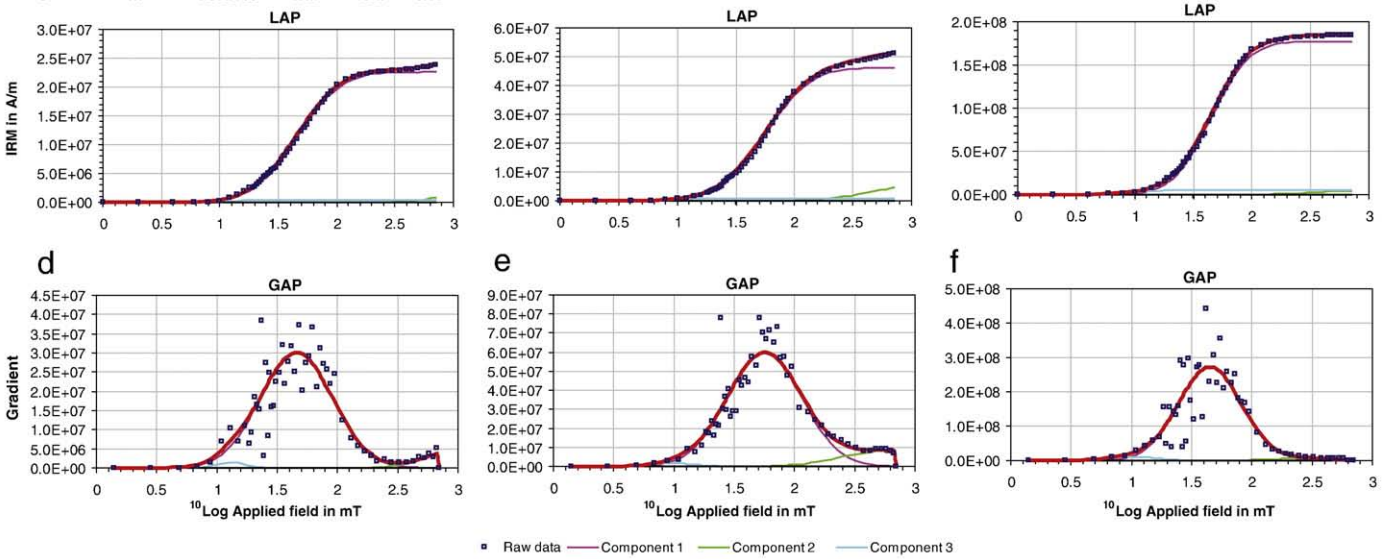

Raw data — Component 1 — Component 2 — Component 3

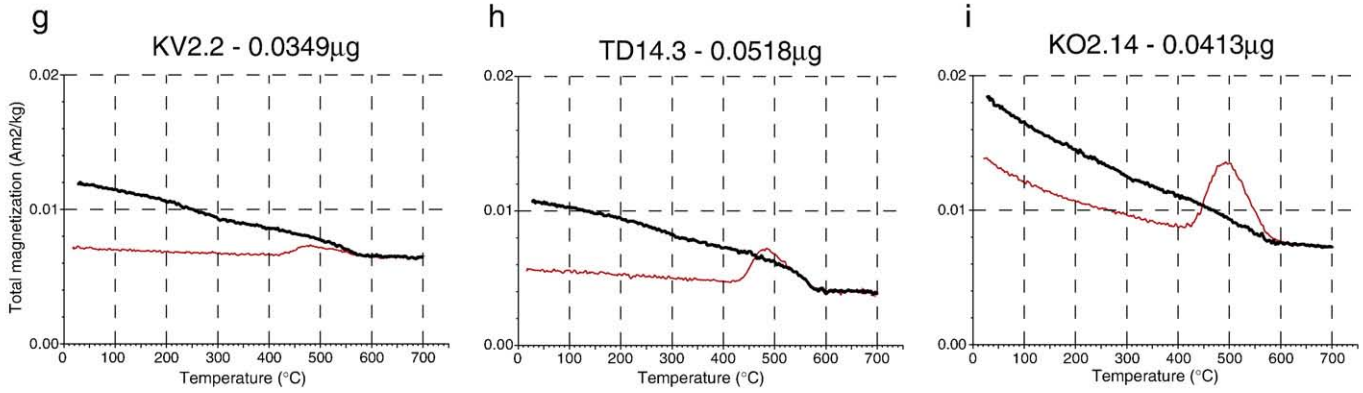

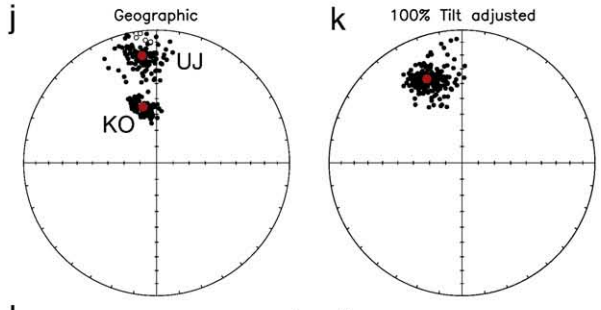

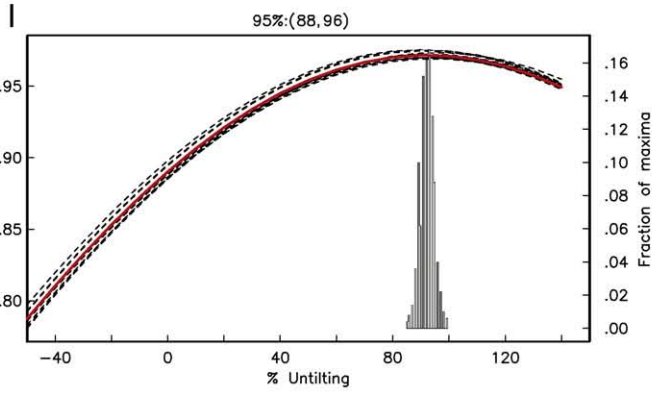

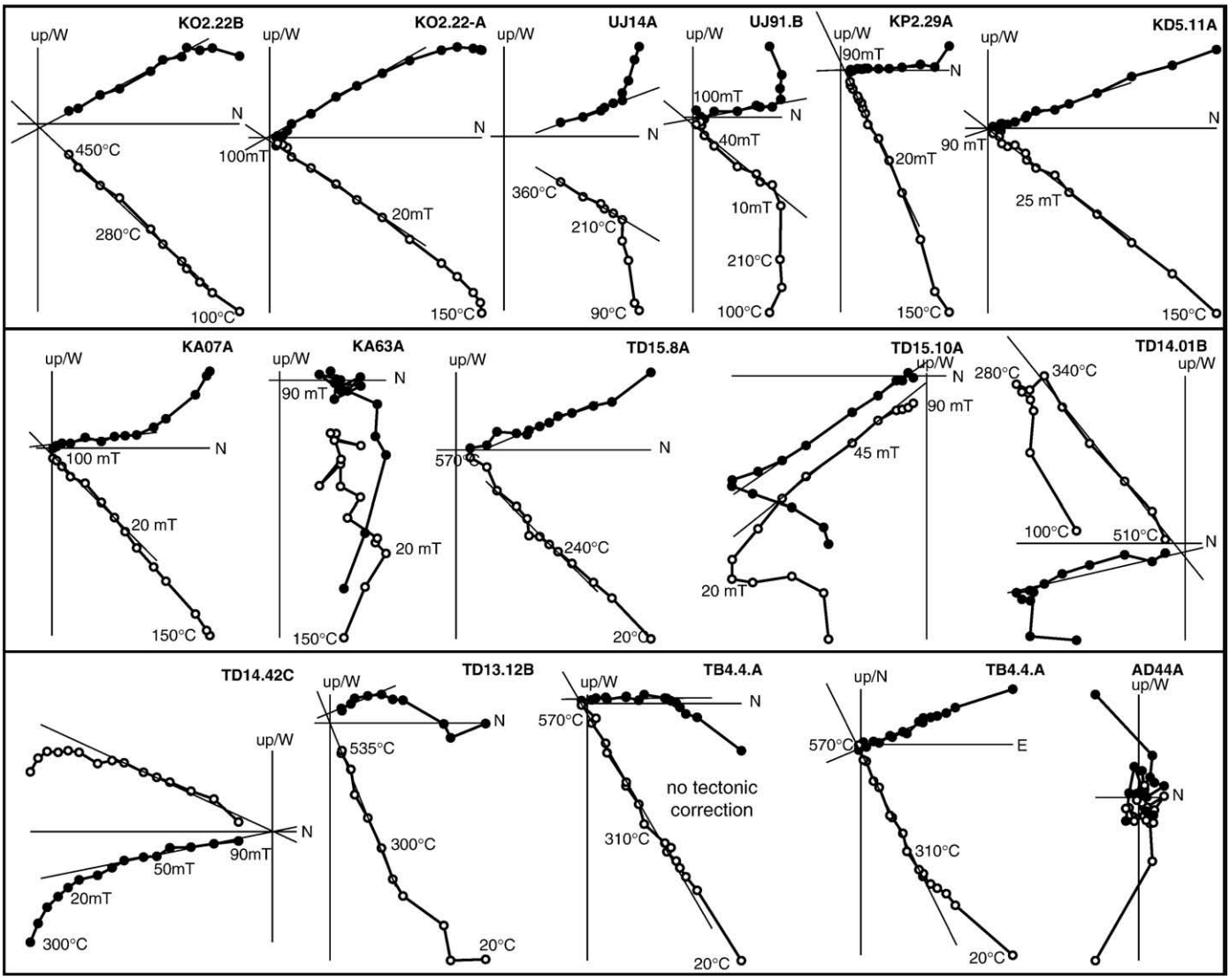

Fig. 3. Orthogonal vector diagrams (Zijderveld, 1967), showing characteristic demagnetization diagrams for sampled sites. Closed (open) circles indicate the projection on the horizontal (vertical) plane. Alternating field and thermal demagnetization steps are indicated. All diagrams (except for TB4.4A notc) are displayed after correction for bedding orientation. For site TD15 we only took the thermally demagnetized samples into account (see Supplementary data).

of (Tauxe and Kent, 2004), which is based on the field model TK03.GAD (Fig. 5, Table 1). The model is based on the assumption that the field averaged over sufficient time resembles that of a geocentric axial dipole (GAD). A large number (preferably $N>100$) of individual directions is required to apply the model successfully. We ran the model for each dataset twice: once without applying a cut-off before running the model, and once applying a variable cut-off (Vandamme, 1994) before applying the model to remove outliers. The difference between both runs was not significant (Table 1).

Our data were compared to the paleolatitudes calculated from the APW paths of Torsvik et al. (2008) and Besse and Courtillot (2002) (Fig. 6), that are very comparable for periods younger than 160 Ma. We discuss results in more detail (per site) in the Supplementary data.

4.2. Reliability criteria

To guarantee the quality of both published and new datasets and to reliably reconstruct the paleolatitude of Crimea and the Pontides throughout the Jurassic and Cretaceous we applied a number of reliability criteria. The datasets and, if applicable, the reason of exclusion from further analysis is indicated in Tables 1 and 2. More detailed information of each site is given in the Supplementary data.

The following reliability criteria were applied:

1) Samples that were demagnetized using bulk demagnetization were excluded, for example sites G1–G5 and O1–O2 in the study of Orbay and Bayburdi (1979),

Fig. 2. a)–f) Examples of IRM component analysis for three sites that were accepted for this study (Kruiver et al., 2001). A legend for the linear acquisition plots (LAP) and gradient acquisition plots (GAP) is given in the figure. The three distinguished components and their contributions, saturation IRM (SIRM), $\log(B_{1/2})$, $B_{1/2}$ and DP are indicated in the tables. g)–i) Thermomagnetic curves measured on a Curie balance (Mullender et al., 1993) for the same three sites as the IRM component analysis examples. Red (black) curves indicate the heating (cooling) curves. The IRM curves and thermomagnetic curves indicate that in all three sites the main magnetic carrier is magnetite. j)–l) Non-parametric fold test (Tauxe and Watson, 1994) on sites UJ and KO. j) Equal area plots of the ChRM before correction for bedding tilt (geographic coordinates), and k) after correction for bedding tilt. Results of the fold test l) as 500 bootstrapped examples of the first eigenvalues (τ_1) upon progressive untilting. Above the diagram the 95% bootstrap error is given.

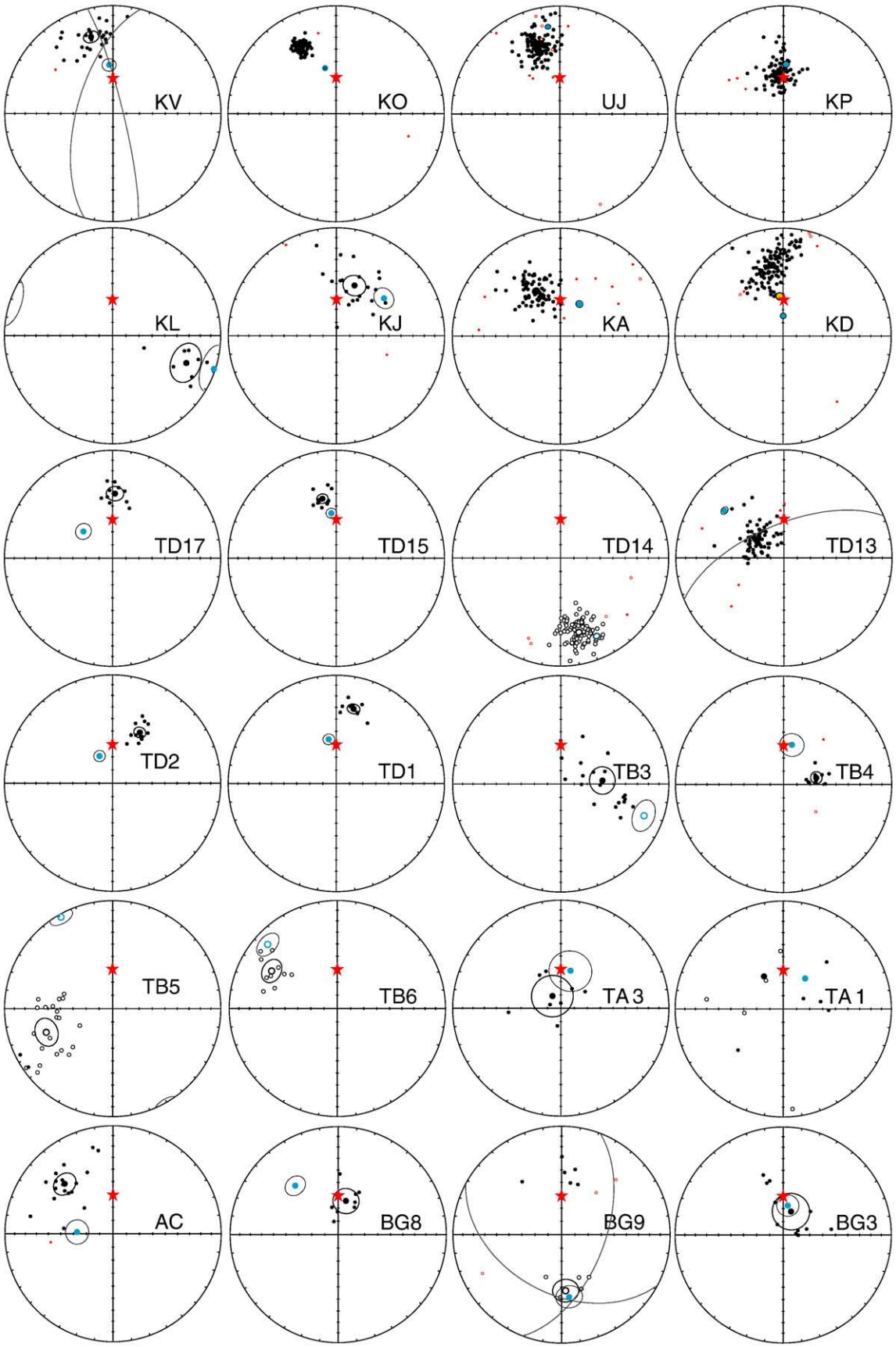
KV
KO
UJ
KP
KL
KJ
KA
KD
TD17
TD15
TD14
TD13
TD2
TD1
TB3
TB4
TB5
TB6
TA 3
TA 1
AC
BG8
BG9
BG3

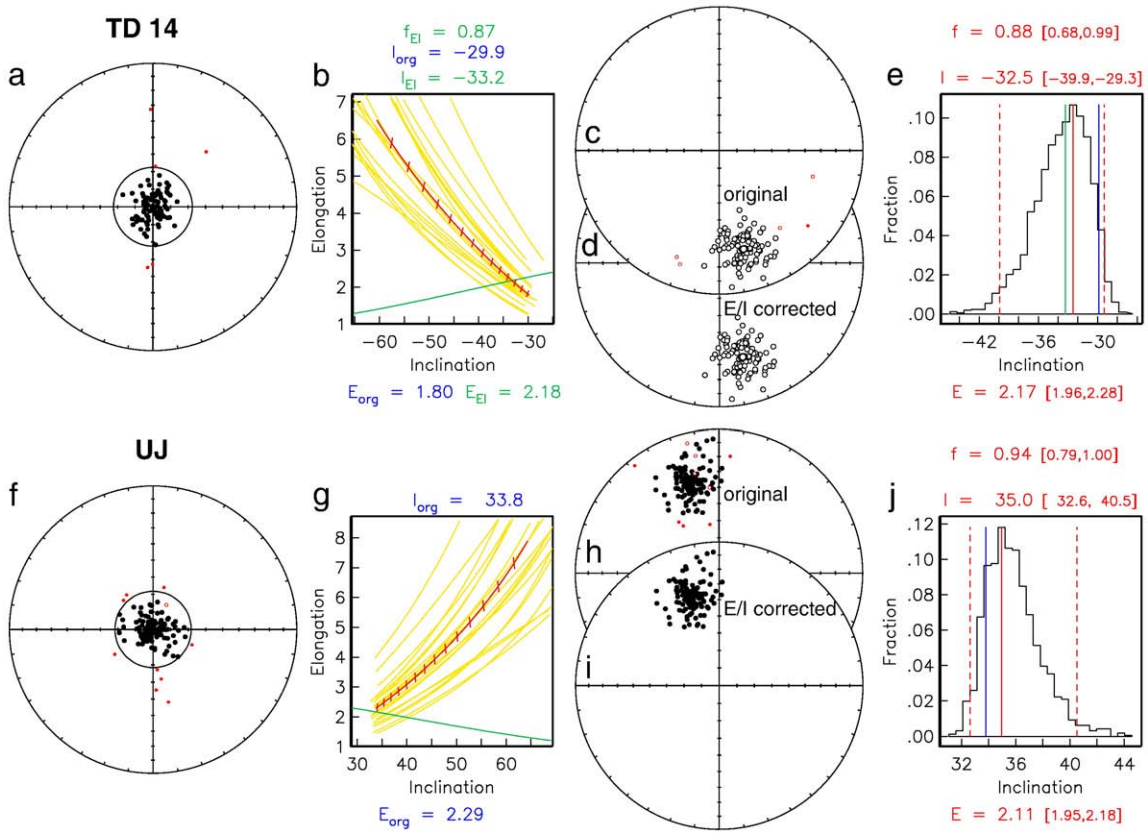

Fig. 5. a)–h) Equal-area projections of the individual VGP directions before *E/I* correction (a and f) and equal-area projections of the individual ChRM directions before (c and h) and after (d and i) *E/I* correction (symbols as in Fig. 4) (Tauxe and Kent, 2004) with corresponding elongation vs. inclination (b and g) and fraction (of 5000 bootstraps) vs. inclination plots (e and j) for TD14 (a–d) and UJ (e–h). In the elongation vs. inclination plots the E/I for the TK03.GAD model (green line) and for the datasets (red barbed line) for different degrees of flattening are plotted. The red barbs indicate the direction of elongation (horizontal is E–W and vertical is N– S). Also shown are examples (yellow lines) from 20 (out of 5000) bootstrapped data sets. The crossing points (if the dataset intersects the model) represent the inclination/elongation pair most consistent with the TK03.GAD model, given as I_{EI} (in green) above the panel; I_{org} = original inclination, E_{org} = original elongation of the dataset, E_{EI} and I_{EI} are the elongation and inclination according to the *E/I* model, respectively. In the fraction/inclination plot, a histogram of intersecting points from 5000 bootstrapped data sets is shown. The most frequent inclination (solid red vertical line; dashed red vertical lines denote the 95% bootstrap error) is given as value (and error range) on top of the panel; the inclinations of the original distribution (blue vertical line) or the intersection with the model (green vertical line) are indicated; *E* = the elongation (and error range) resulting from the bootstrapped data sets.

2) sites that have a mean ChRM direction in geographic coordinates that is indistinguishable from the present-day geocentric axial dipole (GAD) field at the sampling location were excluded,
3) datasets with suspect directions (e.g. N/up or S/down directions) that may result from an insufficiently removed (partial) overprint, datasets with an unresolved component and datasets from sites with samples that were too weak for proper demagnetization resulting in erratic behavior (e.g. TB1), were excluded from further analysis. An example is site TB5, where a temporary problem with the oven that was used for demagnetizing the samples resulted in the acquisition of a spurious component in the samples at higher temperatures (>300 °C). Another example is site TD15 which gave completely different and unexplainable (but consistent) results using AF and thermal demagnetization.
4) datasets with age uncertainties larger than 15 Myrs were excluded,
5) datasets that have an error in latitude (using ΔI_x calculated from A95) that is larger than 7° (averaged over ΔI_x^+ and ΔI_x^-), because this would not give us the resolution to compare the dataset with the APW path,
6) datasets that do not reach the minimum amount of samples ($N>24$) to allow reliable calculation of the paleolatitude (Van der Voo, 1990) were not taken into account. In the case that volcanic rocks were sampled, the minimum required number of flows/sites (with a minimum of demagnetized specimens per lava flow ≥5) that constitute one locality is 5,
7) datasets that do not pass the fold test were excluded. An example of this is site KD, because the six subsets with different bedding orientation do not pass the fold test (of Tauxe and Watson, 1994 (see Supplementary data). The tightest grouping of data occurs at 40% unfolding. We also determined the paleofield direction from a synfolding remanence of site KD using the small circle intersection (SCI) method of Shipunov (1997), modified by Waldhör and Appel (2006) (see Supplementary data). The directions from the foldtest and the SCI method are very comparable. The results suggest that remagnetization occurred at an inclination of 54.6–62.4° (corresponding to a paleolatitude of 35.1°N<38.1°N<43.7°N). If we compare this value to the APW path of Eurasia (Torsvik et al., 2008), this coincides very well with values predicted for post-Paleocene times (Fig. 7), which supports remagnetization, likely during folding.

Fig. 4. Equal area projections of the ChRM directions of all sites except those where $N=0$ (Table 1). Open (closed) symbols denote projection on upper (lower) hemisphere. Large black (blue) symbols with black circle indicate respectively the mean directions and their cone of confidence (α_{95}) after (before) tilt correction. Red (small) circles indicate the individual directions rejected by the Vandamme cut-off angle (Vandamme, 1994). Black lines indicate the great circles that were used to calculate the best fitting ChRM directions (McFadden and McElhinny, 1988). Red star indicates the present-day geocentric axial dipole direction at the sampled location.

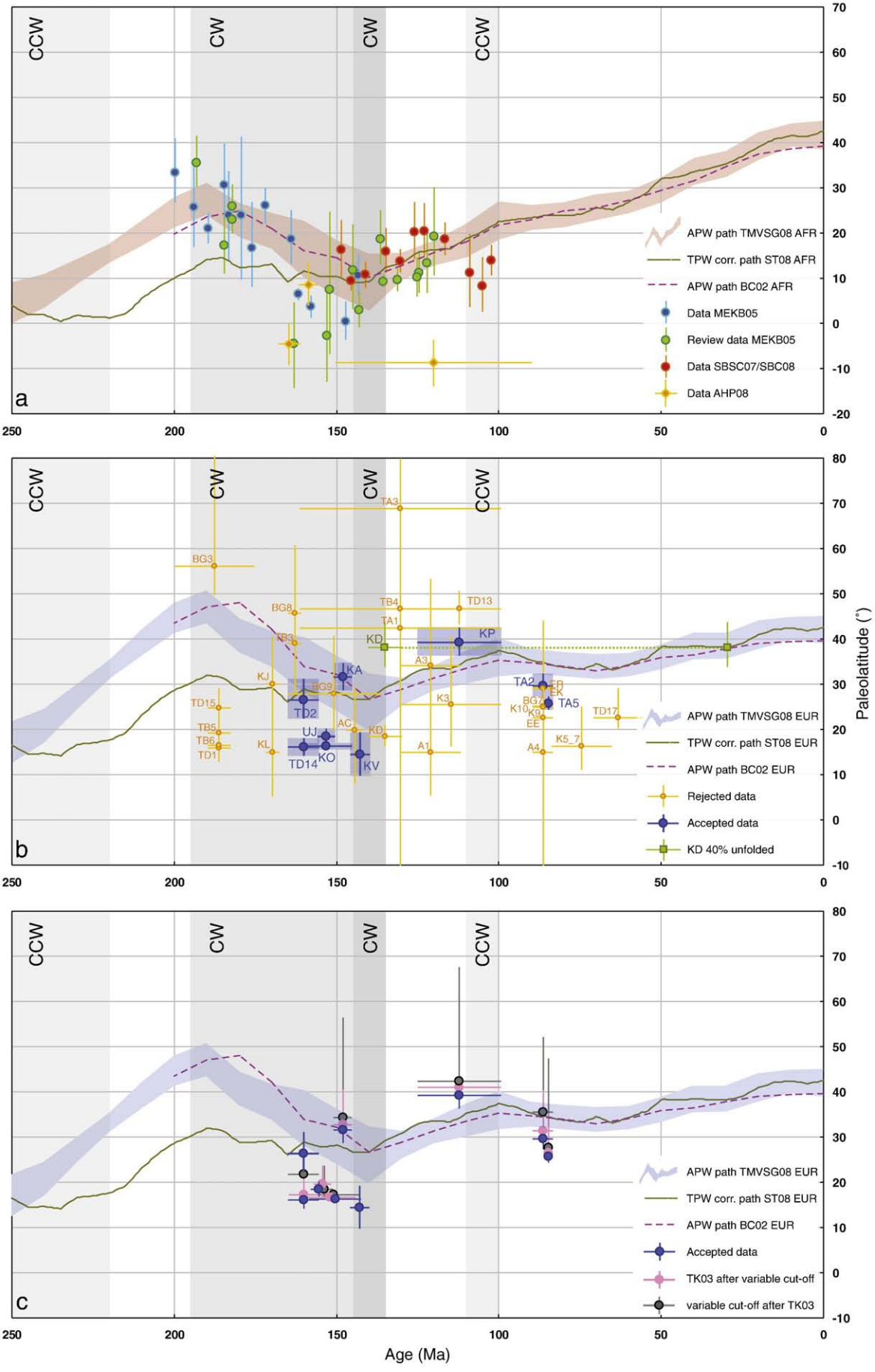
CCW
CW
CW
CCW
a
APW path TMVSG08 AFR
TPW corr. path ST08 AFR
APW path BC02 AFR
Data MEKB05
Review data MEKB05
Data SBSC07/SBC08
Data AHP08
b
APW path TMVSG08 EUR
TPW corr. path ST08 EUR
APW path BC02 EUR
Rejected data
Accepted data
KD 40% unfolded
c
APW path TMVSG08 EUR
TPW corr. path ST08 EUR
APW path BC02 EUR
Accepted data
TK03 after variable cut-off
variable cut-off after TK03
Paleolatitude (°)
Age (Ma)

Table 2
Data from published studies. # = number assigned to the study; *N* (total #) = total number of specimens incorporated in the study; *N* (statistics) = number of combined sites or individual specimens that were used for calculation of the averages and statistics; Δλ+ and Δλ− are the positive and negative latitude errors. Other parameters as for Table 1.

#	Authors	Age	Δ Age	*N* (total #)	*N* (statistics)	Dec	ΔD_x	I_{nc}	ΔI_x	λ	*k*	α_{95}	Δλ+	Δλ−	*K*	A_{95}	Rej
Crimea																	
1	Anferova (1971)	98.5	1.5	13	13	328.4	2.9	58.5	2.0	39.2	600	2	2.3	2.2	352.1	2.2	1, 6
2	Anferova (1971)	134	6	21	21	357.2	10.1	45.1	11.3	26.6	15	9	10.3	8.1	13.4	9.0	1, 5, 6
3	Anferova (1971)	168.5	3.5	18	18	348.2	9.1	45.9	9.9	27.3	22	8	9.1	7.4	19.2	8.1	1, 5, 6
4	Pechersky et al. (1993)	106	6	15	15	349.3	9.2	43.9	10.6	25.7	24.3	7.3	9.3	7.5	22.3	8.3	5, 6
5	Pechersky et al. (1993)	168.5	7.5	48	4	101.6	24.9	30.9	38.1	16.7	13	27	35.9	20.3	15.9	23.8	5
6	Pechersky et al. (1993)	168.5	7.5	22	22	97.4	10.9	43.9	12.5	25.7	12	9	11.3	8.7	11.0	9.8	5, 6
7	Pechersky et al. (1993)	168.5	7.5	43	18	138.6	8.6	45.2	9.5	26.7	24	5	8.5	7.0	21.3	7.7	6
8	Pechersky and Safonov (1993)	161	15	67	5	30.1	3.4	52.5	3.0	33.1	999.9	0.5	3.0	2.8	716.5	2.9	7
9	Pechersky and Safonov (1993)	130.5	30.5	22	2	351.6	61.1	49	56.5	29.9	34.8	4.7	−90.8	33.7	27.8	49.4	6
10	Pechersky and Safonov (1993)	149.5	1.5	21	4	308.1	15.7	44.8	17.6	26.4	49	4.7	17.3	12.0	44.0	14.0	6
11	Pechersky and Safonov (1993)	149.5	1.5	45	2	353.3	16.9	49.6	187.0	30.4	6.8	8	6.7	5.7	5.3	165.4	5
12	Pechersky and Safonov (1993)	155.5	2.5	19	2	326	33.9	41.4	41.2	23.8	69.8	3.9	51.7	23.7	68.4	30.7	6
13	Pechersky and Safonov (1993)	158	5	52	4	352.1	10.5	45.7	11.5	27.1	112.4	6.6	10.6	8.3	98.5	9.3	6
14	Pechersky and Safonov (1993)	168.5	7.5	34	2	121.9	>90	43.1	92.8	25.1	15.4	6.2	50.9	55.6	14.5	71.4	6
15	Pechersky and Safonov (1993)	168.5	3.5	28	28	31.8	7.6	40.6	9.6	23.2	16.1	6.6	7.7	6.5	16.1	7.0	5
16	Pechersky and Safonov (1993)	148.5	2.5	8	8	329.5	16.7	36	23.3	20.0	12.1	14.3	20.1	13.5	13.4	15.7	5, 6, 7
17	Pechersky and Safonov (1993)	149.5	1.5	7	7	357.1	12.2	61	7.7	42.1	84.8	5.7	10.0	8.2	45.6	9.0	5,6,7
18	Pechersky and Safonov (1993)	145.5	5.5	10	10	343.2	14.5	49.3	14.3	30.2	20	5.3	15.0	10.9	15.8	12.5	5, 6, 7
19	Pechersky and Safonov (1993)	153.5	7.5	17	17	5.3	6.4	54.4	5.3	34.9	70.1	5.6	5.6	4.9	47.3	5.2	7
20	Anferova (1971)	115.5	9.5	216	5	1	11.0	48.6	11.1	29.6	80	9	11.0	8.6	64.6	9.6	1
21	Pechersky and Safonov (1993)	149.5	1.5	66	3	347.7	17.1	32.7	25.5	17.8	49.2	11.5	21.1	14.2	58.2	16.3	
22	Rusakov (1971)	118.5	6.5	37	37	357.2	5.7	68.9	2.4	52.3	116	2	3.6	3.4	46.8	3.5	See text
Pontides																	
23	Van der Voo (1968)	77.4	11.9	6	6	343.6	8.4	44.7	9.4	26.3	90	7	8.3	6.8	81.0	7.5	5, 6
24*	Saribudak (1989)	86.4	2.9	57	7	349.5	13.2	41.9	16.0	24.2	27	11.8	14.4	10.5	26.1	12.0	5
25	Van der Voo (1968)	173	27	8	8	320.9	6.3	10.1	12.2	5.1	51	8	6.5	6.2	79.3	6.3	6
26	Van der Voo (1968)	48.1	7.7	16	16	317	7.2	41.4	8.9	23.8	33	16	7.2	6.1	32.3	6.6	6
27	Saribudak (1989)	114.8	15.2	5	5	2.6	4.4	−2	8.8	1.0	190	5.6	2.4	6.4	303.7	4.4	4, 6
28**	Orbay and Bayburdi (1979)	83	17.5	7	7	343.8	16.7	54.4	13.7	34.9	30.6	9.6	16.3	11.7	20.6	13.6	1, 2?, 5, 6
29	Van der Voo (1968)	180.4	19.2	6	6	330.7	13.5	44.4	15.3	26.1	35	11	14.4	10.5	31.8	12.1	5, 6
30	Evans et al. (1982)	161	15	134	134	95.1	12.2	53.4	10.5	33.9	3.5	7.7	11.7	9.0	2.4	10.1	3, 5
31	Channell et al. (1996) group 1	86.4	2.9	59	5	336.3	6.8	43	8.0	25.0	166.4	5.9	6.7	5.7	156.6	6.1	Incl. in # 36
32	Channell et al. (1996) group 2	86.4	2.9	47	3	325	20.1	46.9	21.2	28.1	58.7	16.2	23.1	14.6	49.7	17.7	Incl. in # 36
33	Channell et al. (1996) group 3	86.4	2.9	116	9	328.1	7.5	43.4	8.8	25.3	62.2	6.6	7.5	6.3	57.9	6.8	Incl. in # 36
34	Channell et al. (1996) group 4	86.4	2.9	71	6	355	13.2	41.3	16.2	23.7	32.4	11.9	14.5	10.6	31.8	12.1	Incl. in # 36
35	Channell et al. (1996) group 5	86.4	2.9	63	5	7.8	19.9	40.6	24.9	23.2	18.5	18.3	24.5	15.2	18.5	18.3	Incl. in # 36
36* **	**Channell et al. (1996) group 1–5**	**86.4**	**2.9**	**356**	**5**		**3.0**	**41.1**	**3.8**	**23.6**	**765.4**	**2.4**	**2.9**	**2.7**	**755.3**	**2.8**	
37	Channell et al. (1996) group 6	86.4	2.9	69	5	91.2	35.1	32.8	51.8	17.9	5.3	36.7	61.4	27.6	6.3	33.2	4
38	Channell et al. (1996) group 7/8	187.6	12	101	9	351.4	23.7	65.8	11.7	48.0	26.3	10.2	18.1	13.4	11.9	15.6	Incl. in # 39
39* **	**Channell et al. (1996) group 7/8**	**187.6**	**12**	**101**	**9**		**7.5**	**60.5**	**4.8**	**41.5**	**155.9**	**4.1**	**6.0**	**5.3**	**85.3**	**5.6**	
40	Channell et al. (1996) group 8/9	86.4	2.9	58	6	354.7	14.0	46.9	14.8	28.1	36.2	11.3	14.7	10.7	30.7	12.3	Incl. in # 42
41	Channell et al. (1996) group 10	86.4	2.9	119	10	349.7	10.1	46.3	10.9	27.6	35	8.3	10.2	8.0	30.2	8.9	Incl. in # 42
42* **	**Channell et al. (1996) group 8/9–10**	**86.4**	**2.9**	**177**	**16**		**6.7**	**43.7**	**7.8**	**25.5**	**40.9**	**5.8**	**6.6**	**5.6**	**37.8**	**6.1**	
43	Channell et al. (1996) group 11/12	180.4	19.2	49	3	21.7	>90	65.5	60.6	47.7	7.6	48.3	−82.1	45.2	3.5	79.9	4

*For the average of Saribudak (1989) (study 24), only seven of the eight published sites were used, as was entered in the GPMDB, namely GO01–06, CI01, BA01, ER01, DE01,SI01, SI02 (so without KA01).
**The average of Orbay and Bayburdi (1979) (study 28) was based on sites G1–G5 and O1–O2.
***The combined inclination-only datasets were calculated by Channell et al. (1996) to a reference point at 41°N, 36°E.

We rejected site TD13 and the site in Crimean sediments from Rusakov (1971), because the inclination of the reported data is, even when taking the error into account, higher than the present-day GAD field inclination at the sampling locality. Two sites with the same age that were sampled in close proximity within the same sedimentary sequence were rejected, because their mean ChRM directions are very different (site KL and KJ, see Supplementary data).

Fig. 6. a) Blue/yellow/red circles (with Δλ error bars calculated from the ΔI_x) respectively from the studies by Muttoni et al. (2005), Aiello et al. (2008) and Satolli et al. (2007; 2008). Green circles (with their Δλ error bars calculated from the ΔI_x) or dp/dm error bars: literature data used in the reconstruction by Muttoni et al. (2005). All data from Adria were recalculated to 42.5°N,31°E. More information about the data: see Section 6. MEKB05: Muttoni et al. (2005); SBSC07: Satolli et al. (2007); SBC08: Satolli et al. (2008); AHP08: Aiello et al. (2008). b) Small yellow (large blue) circles (with Δλ error bars calculated from the ΔI_x) and age error bars: rejected (accepted) data from this study. Green squares with Δλ error bars calculated from the ΔI_x and age error bars indicate the paleolatitude of site KD after 40% unfolding, green dotted line shows the path along a fixed paleolatitude until it intersects the APW path, indicating the possible moment of remagnetization. c) Blue large circles as in Fig. 7b; pink large circles: data after correction with the *E*/*I* method (Tauxe and Kent, 2004) on which a variable cut-off has been applied (Vandamme, 1994) prior to *E*/*I* correction, with the 95% bootstrap error range; grey large circles: data after correction with the *E*/*I* method (Tauxe and Kent, 2004) on which a variable cut-off has been applied (Vandamme, 1994) after *E*/*I* correction. The *E*/*I* correction was only applied on sufficiently large data sets. The ages of two sites (KO and UJ) were shifted slightly for readability. In all three panels the shaded areas show the age versus latitude plot for our reference location calculated from the African (in pink, Fig. 6a) or Eurasian (in blue, Fig. 6b–c) APW paths of (Torsvik et al., 2008), calculated for 42.5°N, 31°E. A 95% confidence level (Δλ error envelope) was calculated from ΔI_x. The age versus latitude calculated from Besse and Courtillot (2002) are indicated as dashed curves from 200–0 Ma. Latitudes derived from the TPW corrected APW path of Steinberger and Torsvik (2008) are indicated as a green solid curve (250–0 Ma) for the African paths (Fig. 6a) and the Eurasian paths (Fig. 6b). Grey shaded areas in all three panels indicate the periods of true polar wander and the sense of motion it would cause in the circum-Black Sea area, calculated by Steinberger and Torsvik (2008). CCW: counterclockwise; CW: clockwise; TMVSG08: Torsvik et al. (2008); ST08: Steinberger and Torsvik (2008); BC02: Besse and Courtillot (2002). We did not correct for relative motion between the Pontides and Crimea, because the relative motion since the Late Jurassic would be on the order of a few degrees, which is well within paleomagnetic errors.

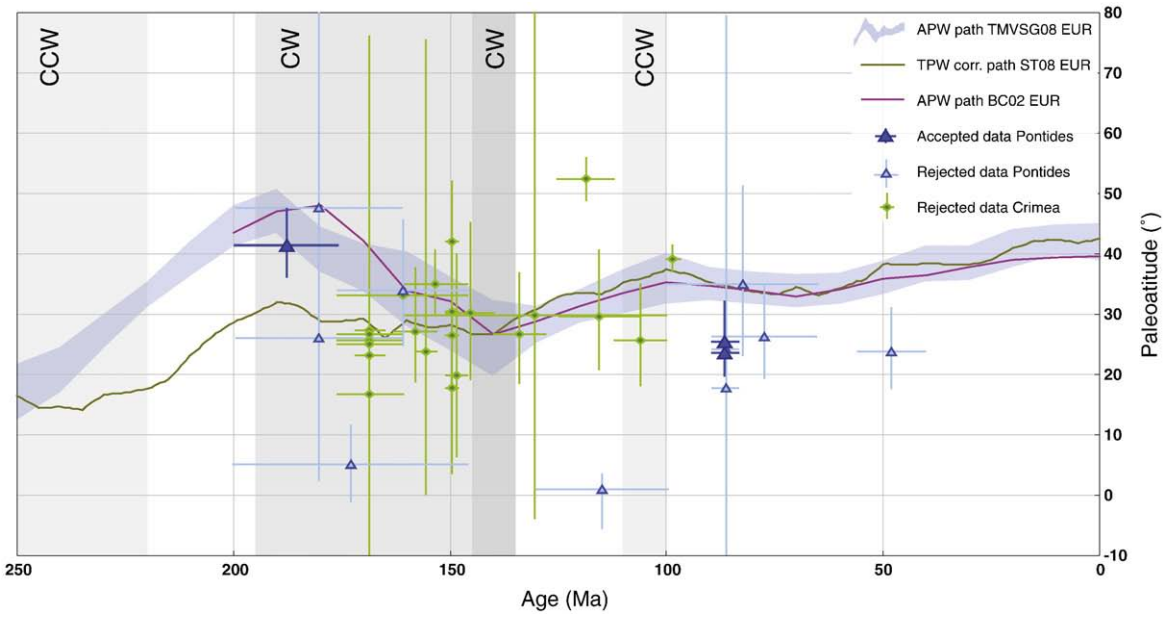

Fig. 7. Literature data from the Pontides and Crimea. Blue shaded area: age versus latitude plot of the Eurasian APW path and its Δλ error envelope calculated from the ΔI_x error envelope of Torsvik et al. (2008) (blue shaded area, 250–0 Ma), age versus latitude plot calculated from the EurasianAPW path of Besse and Courtillot (2002) (purple curve, from 200 to 0 Ma) and calculated from the Eurasian TPW corrected APW path of Steinberger and Torsvik (2008) (green curve, 250–0 Ma). Small green diamonds (small blue triangles): rejected data from the GPMDB data from Crimea (Pontides); large blue triangles: accepted data from the GPMDN data from the Pontides. In the data for the Pontides, also data from Channell et al. (1996) were included. The data from Channell et al. (1996) are the only accepted data. No Crimean data passed our reliability criteria. All Δλ error bars were calculated from the ΔI_x (95% confidence level). Horizontal error bars: age errors. All data were recalculated to a reference point in the Black Sea region (42.5°N, 31°E). Abbreviations in legend as in Fig. 6.

5. Results

5.1. Results — this study

After applying the above reliability criteria, there are nine remaining datasets from the 41 datasets for the paleolatitude reconstruction of Crimea and the Pontides in Jurassic–Cretaceous times. The nine remaining datasets are from three age ranges: Callovian–Berriasian (~164.7–140.2 Ma, six sites), Aptian–Albian (~125.0–99.6 Ma, one site) and Coniacian–Santonian (~89.3–83.5 Ma, two sites) (Fig. 6b; Table 1, indicated in bold face). The oldest interval consists of datasets from both Crimea and the Pontides; the middle age interval contains only Crimean data, and the youngest interval consists only of datasets from the Pontides.

Two of our datasets that were taken from Upper Jurassic rocks have similar ages: sites UJ and KO. Because of their proximity and the difference in bedding tilt, we performed a fold test. The equal-area plots of directions from both limbs before and after tilt correction (Fig. 2j–l) show that in geographic coordinates the two sites have significantly different directions, while after tectonic tilt correction the directions of both sites form a single cluster. The nonparametric fold test of Tauxe and Watson (1994) (Fig. 2j–l) is considered to be positive because closest grouping is reached close to full unfolding (95% bootstrap errors: 88%–96%). The small deviation from 100% significance may be caused by orientation or bedding plane errors. This fold test checks for maximum clustering, but this need not always be the ideal case (McFadden, 1998), while also a well-recorded secular variation distribution would have a slight elongation at this latitude, which is not necessarily compatible with maximum clustering. Furthermore, the two groups of pre-untilting directions that can be seen within the data of site KO (Fig. 2j), and that form one cluster after tectonic tilt correction (Fig. 4), give an extra indication that the ChRM direction is a pre-folding direction. Hence, we conclude that the magnetization of site UJ and KO was acquired before folding, even though the tilt corrected means just fail to have a common true mean direction (ctmd). To determine whether two distributions have a ctmd, we used the reversal test developed by McFadden and McElhinny (1990) and their classifications (A, B, C, indeterminate). The classifications are based on the critical angle γ_c and the angle γ between the means. Because we use their test with simulation, the test is equivalent to using the V_w statistical parameter of Watson (1983).

In the oldest interval (~164.7–140.2 Ma), we have six datasets (two from the Pontides and four from Crimea); four of these were corrected for inclination error with the *E/I* method (Tauxe and Kent, 2004). The *E/I* method was carried out on the datasets before and after applying a variable cut-off to the datasets (Vandamme, 1994) (see Section 4.1). The difference between both approaches is negligible (Fig. 6), on average the calculated paleolatitude correction after applying the E/I method is not significant and only ~2–3° higher than before applying the method (Fig. 5). In the oldest age interval, when not taking into account site KA that yields a higher paleolatitude (~31°N) than the other sites, a trend through all other datasets can be observed that is consistent with the APW path (decreasing from ~21°N at ~165 Ma to ~16°N at ~140 Ma) (Fig. 6).

From the five sites that were sampled in rocks from intervals (overlapping) the Aptian–Albian (~125.0–99.6 Ma), one site from Crimea (KP) passed the reliability criteria. Site KP yields a paleolatitude that is within error (ΔI_x and age error) with the paleolatitude predicted by the APW paths (Besse and Courtillot, 2002; Torsvik et al., 2008), before and after correction with the *E/I* method. Unfortunately, the site has a relatively large age error (±12.7 Ma).

The two datasets from the Pontides from the youngest age group (~89.3–83.5 Ma) yield paleolatitudes that are very comparable (TA2) to slightly lower (TA5) than the paleolatitudes that are predicted by the APW paths (Besse and Courtillot, 2002; Torsvik et al., 2008), both before and after correction with the E/I method.

5.2. Results — literature data

All data reported for the area of interest from the global paleomagnetic database (GPMDB) (Smethurst, 2009) are listed in Table 2 and shown in Fig. 7. The studies in the GPMDB are from Van der Voo (1968), Anferova (1971), Rusakov (1971), Orbay and Bayburdi (1979), Evans et al. (1982), Pechersky and Safonov (1993) and Pechersky et al. (1993). A full author list could not be traced for Pechersky et al. (1993). We added the data of

Channell et al. (1996) to this review, because they are not part of the GPMDB. Many of the published data were rejected after applying the reliability criteria. For the Pontides, only three out of 13 results were accepted, all three from the combined results of Channell et al. (1996). None of the 22 Crimean datasets passed the reliability criteria. All sites that passed the reliability criteria are indicated in bold face in Table 2.

A major problem with the Crimean data in the database is that they can often not be traced back to the original publication. In some cases, the k (precision parameter), α_{95} values and number of samples of datasets that were combined in the GPMDB do not coincide with our calculations. The number of samples used for the calculations also differed sometimes between the paper and the database. In one case, a

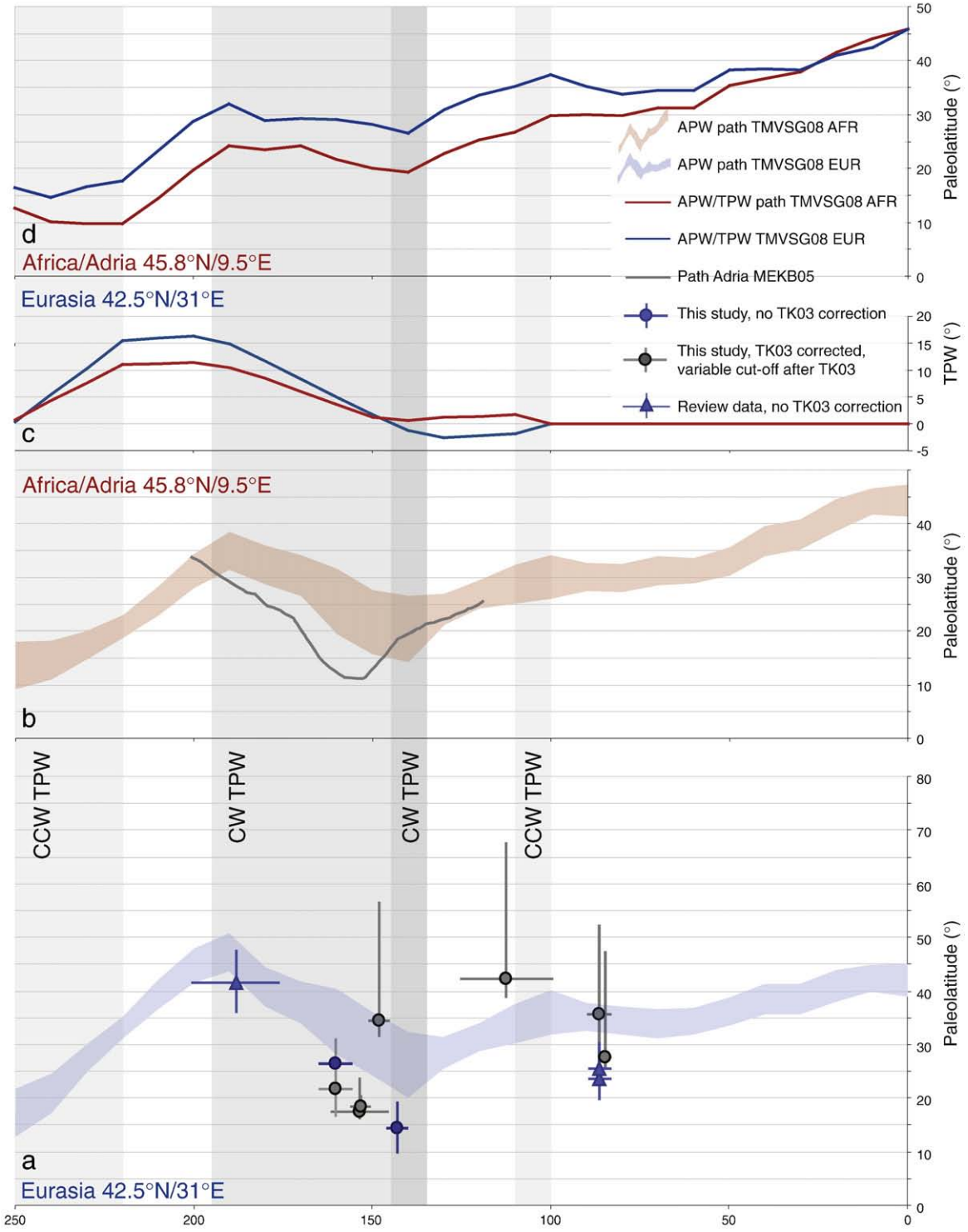

Fig. 8. a) and b) Age versus latitude plot calculated from the Eurasian (African) APW path and its $\Delta\lambda$ error envelope calculated from the ΔI_x error given by Torsvik et al. (2008) (blue (red) shaded area, 250–0 Ma). a) blue large circles as in Fig. 6b; grey large circles as in Fig. 6c, blue triangles: literature data from Channell et al. (1996) (as in Fig. 7). The *E*/*I* correction was only applied to sufficiently large data sets. b) Grey curve: curve calculated by Muttoni et al. (2005). c) Curve indicating the amount of TPW through time for the African (in red) and Eurasian (in blue) continents. d) Age versus latitude plot calculated from the TPW corrected APW paths for Africa (in red) and Eurasia (in blue) from Steinberger and Torsvik (2008). All paths and datapoints are recalculated to the locations indicated in the figure. Abbreviations in legend as in Fig. 6.

single dataset was entered three times into the database, under different authors, and combined with several other sub-datasets.

6. Discussion

Data from five out of six sites from Callovian–Berriasian (~164.7–140.2 Ma) rocks show very consistent behavior and suggest that the Pontides (sites TD14, TD2) and Crimea (sites KO, UJ, and KV) were not situated at significantly different latitudes in Late Jurassic times (Figs. 6 and 8), which would imply close vicinity of the Pontides and Crimea in this period. Therefore, even if there was an oceanic basin separating the Pontides and Crimea in this time span, it was of limited dimension (no more than several hundred of km). Our data (except site KA) yield paleolatitudes that are significantly lower (~1600 km) than the paleolatitude expected from the APW paths of Besse and Courtillot (2002) and Torsvik et al. (2008). The consistent low paleolatitudes from Callovian to Berriasian (~164.7–140.2 Ma) rocks from Pontides and Crimea, show a southward moving trend (Figs. 6 and 8), which is near-parallel to the trends in the Eurasian APW paths (Besse and Courtillot, 2002; Torsvik et al., 2008) in the same interval.

Data from Aptian–Albian (~125.0–99.6 Ma) rocks from Crimea (site KP) yield a paleolatitude that are slightly higher than the paleolatitudes predicted by the APW paths, but identical within error (Fig. 6b, blue shaded area), both before and after correction with the *E/I* method (Figs. 6 and 8, Table 1). Coniacian–Santonian (~89.3–83.5 Ma) data from the Pontides from site TA5 reveal a paleolatitude that, after correction with the *E/I* method, plot on the APW path, whereas the paleolatitude from site TA2 are slightly lower, but within error, to the Late Cretaceous APW paths (Besse and Courtillot, 2002; Torsvik et al., 2008). The datasets from Upper Cretaceous formations published by Channell et al. (1996) however, yield slightly lower latitudes than predicted by the APW paths. This could be the result of inclination shallowing, because the data were not corrected for this. The accepted site of Liassic age from Channell et al. (1996) plots within error of the APW path.

Our low latitudes in Middle Jurassic to Early Cretaceous times, compared to the Eurasian APW paths, are in line with the low latitudes of Adria as part of the African plate, presented in the study of Muttoni et al. (2005). On the basis of a magnetostratigraphic study on sections in the Northern Apennines (Italy), Satolli et al. (2007; 2008) calculated a pole path for Adria for the ~100–150 Ma interval. We used their poles to calculate the paleolatitude at our reference location (Fig. 6a). The paleolatitudes derived from their study in the ~125–145 Ma interval are in line with the data presented by Muttoni et al. (2005). However, in the critical interval prior to 145 Ma that displays the southward movement of Africa, their calculated paleolatitude is higher than predicted by the scenario of Muttoni et al. (2005), and comparable to the APW paths. Therefore, they disagree with Muttoni et al.'s (2005) scenario of a more southerly position of Africa in the Middle to Late Jurassic times, compared to the APW paths. One datapoint from a study by Aiello et al. (2008) on Greek radiolarian cherts that has a small age error (<5 Myr, Fig. 6) yields also a paleolatitude that is much lower than expected from the African APW path, the other data point yields a slightly lower paleolatitude. In the critical interval the sampled localities are also a part of the African plate (Fig. 1b). In general the data from Aiello et al. (2008) from Greek radiolarian cherts support the scenario of Muttoni et al. (2005). The data from Aiello et al. (2008) do however not pass our reliability criteria due to too large age errors and too small datasets (Fig. 6a).

Muttoni et al. (2005) conclude that the southward movement and clockwise motion of Africa is underestimated by the APW path of Besse and Courtillot (2002) because of smoothing of the data. This discrepancy remains if their results are compared to the pole path of Torsvik et al. (2008), because both paths are nearly identical from the start of the critical time interval (~160 Ma) onwards (Figs. 6–8). Smoothing seems a likely mechanism, because of the relatively low amount of data entries in the global APW path of Torsvik et al. (2008): the average number of data entries per 10 Myr sliding window in the pole path is 27 (320–0 Ma), whereas this is only 13 in the critical time span (160–140 Ma). The pole path calculated by Satolli et al. (2008) does not support Muttoni's scenario, but in their study they do recognize an abrupt change in plate movement direction around ~141 Ma. Therefore, Satolli et al (2007) propose the possibility of TPW in this time span.

From our six datasets from Upper Jurassic to Early Cretaceous rocks that were deposited at the southern Eurasian margin, five do show a ~1600 km lower paleolatitude than expected from the Eurasian APW paths, out of which four yield a paleolatitude that is statistically significantly lower than the APW path (TD14, KO, UJ and KV) (Figs. 6c and 8a). This suggests that Muttoni et al.'s (2005) scenario wherein the southward movement of the African APW paths is underestimated, seems not only valid for Africa, but also for Eurasia. The fact that datasets from other pre- and post-TPW Jurassic and Cretaceous periods from the Pontides and Crimea (Fig. 8) plot within error on the APW path except for two sites that were not corrected for inclination error, confirms that we have a good control on paleolatitude. Because Africa and Eurasia were separated and partly surrounded by subduction zones, which serve as an anchor into the mantle, it is unlikely that both plates moved ~1600 km back and forth with respect to the mantle (Fig. 1b). Therefore, we conclude that the latitudinal shift is most likely the result of TPW. We concur with Muttoni et al. (2005) that the strong southward movement, followed by a northward movement in the APW paths is smoothed, and because these smoothed paths were used to calculate the TPW events by Steinberger and Torsvik (2008), the Jurassic TPW event was probably larger than determined so far.

7. Conclusions

Here, we tested whether recently published Jurassic to Early Cretaceous large southward movements, followed by northward movements of the African plate at the position of Adria can also be found on the Eurasian plate in the present-day circum-Black Sea area. We have presented large paleomagnetic datasets (41) from Jurassic and Cretaceous sediments from Crimea (Ukraine) and the Pontides (Turkey) that were part of the Eurasian plate. To correct for inclination error in sediments, we used the statistical *E/I* method of Tauxe and Kent on datasets with a sufficient number of samples. Our data were combined with 43 published datasets. After applying strict reliability criteria on all 84 datasets, only 12 datasets were accepted. Five out of six Late Jurassic to Early Cretaceous datasets plot on average ~1600 km lower than the paleolatitudes calculated by the Eurasian APW paths confirming that the southward movement of Africa is also observed in Eurasia. Moreover, the datasets from Crimea and the Pontides display very similar paleolatitudes in this time span, and therefore imply their proximity in the Late Jurassic to Early Cretaceous.

The weaker signature of this southward movement, followed by a northward movement in the APW paths, can result from data smoothing. This is very likely for a period with a low amount of high quality datasets and a sharp change in motion.

There are two mechanisms to explain this southward translation of the Eurasian and African plates in the eastern Mediterranean realm: 1) movement of the African and Eurasian plates with respect to the surrounding plates, 2) movement of the entire crust and mantle with respect to the Earth's core: true polar wander (TPW), recently quantified by Steinberger and Torsvik (2008) for the critical time span. Because it is unlikely that Africa and Eurasia moved with such high speed with respect to the surrounding plates in a time span where both continents were surrounded by subduction zones, wherein the subducting slabs function as their anchors in the mantle, we regard the possibility of TPW the most likely mechanism to explain the low latitudes.

Acknowledgements

The authors would like to thank Nuretdin Kaymakcı for discussion. We would like to acknowledge the following people for their help in the

field: Wout Krijgsman, Martijn Deenen, Aline Saintot, Stephen Vincent, Vladimir Bakhmutov, Sergei Bolotov, Oleg Rusakov, Evgeniy Polyachenko, Galina Slivinskaya, Sergei Yudin, Elena Yudina, Viktor Yudin, Aral Okay, Nuretdin Kaymakcı, Bora Rojay, Pinar Ertepınar Kaymakcı and Ane Wiersma. V.V. Arkadiev is thanked for age determination of Crimean ammonite samples. We would like to thank Bernhard Steinberger for providing the Eurasian and African TPW-corrected paths. We would like to thank Aral Okay, Rob van der Voo and two anonymous reviewers for their constructive comments. M.J.M.M. acknowledges The Netherlands Research Centre for Integrated Solid Earth Sciences (ISES) and The Netherlands Organization for Scientific Research (NWO) for financial support. D.J.J.v.H. acknowledges financial support from Statoil (SPlates project). The global paleomagnetic database can be found at: http://www.ngu.no/geodynamics/gpmdb/.

Appendix A. Supplementary data

Supplementary data associated with this article can be found, in the online version, at doi: 10.1016/j.epsl.2010.04.052.

References

Aiello, I.W., Hagstrum, J.T., Principi, G., 2008. Peri-equatorial paleolatitudes for Jurassic radiolarian cherts of Greece. Tectonophysics 448, 33–48.
Altıner, D., Koçyiğit, A., Farinacci, A., Nicosia, U., Conti, M.A., 1991. Jurassic–lower Cretaceous stratigraphy and paleogeographic evolution of the southern part of north-western Anatolia (Turkey). Geologica Romana 27, 13–80.
Anferova, K.I., 1971. Paleomagnetic directions and pole positions: Data for the USSR, 1. Soviet Geophysical Committee: World data Center-B, Moscow.
Banks, C.J., Robinson, A.G., 1997. Mesozoic strike–slip back-arc basins of the western Black Sea region. In: Robinson, A.G. (Ed.), Regional and Petroleum Geology of the Black Sea and Surrounding Regions, 68. AAPG Memoir, pp. 53–62.
Banks, C.J., Robinson, A.G., Williams, M.P., 1997. Structure and regional tectonics of the Achara–Trialet fold belt and the adjacent Rioni and Kartli foreland basins, Republic of Georgia. In: Robinson, A.G. (Ed.), Regional and Petroleum Geology of the Black Sea and Surrounding Region, 68. AAPG Memoir, pp. 331–346.
Barrier, E., Vrielynck, B., 2008. Paleotectonic maps of the Middle East. Middle East Basins Evolution Programme, CCGM–CGMW, Paris.
Besse, J., Courtillot, V.E., 1991. Revised and synthetic apparent Polar Wander paths of the African, Eurasian, North American and Indian Plates, and True Polar Wander since 200 Ma. Journal of Geophysical Research 96, 4029–4050.
Besse, J., Courtillot, V., 2002. Apparent and true polar wander and the geometry of the geomagnetic field in the last 200 million years. Journal of Geophysical Research 107 (B11). doi:10.1029/2000JB000050.
Bozkurt, E., Winchester, J.A., Yiğitbaş, E., Ottley, C.J., 2008. Proterozoic ophiolites and mafic–ultramafic complexes marginal to the İstanbul Block: an exotic terrane of Avalonian affinity in NW Turkey. Tectonophysics 461, 240–251.
Butler, R.F. 1992. Paleomagnetism: Magnetic domains to geologic terranes (Eds.), Boston, Blackwell Scientific Publications, pp. 83–104.
Channell, J.E.T., Tüysüz, O., Bektaş, O., Şengör, A.M.C., 1996. Jurassic–Cretaceous paleomagnetism and paleogeography of the Pontides (Turkey). Tectonics 15 (1), 201–212.
Cloetingh, S., Spadini, G., Van Wees, J.D., Beekman, F., 2003. Thermo-mechanical modelling of Black Sea Basin (de)formation. Sedimentary Geology 156, 169–184.
Creer, K.M., Irving, E., Nairn, A.E.M., 1959. Paleomagnetism of the Great Whin Sill. Geophysical Journal of the Royal Astronomical Society 2, 306–323.
Dercourt, J., Gaetani, M., Vrielynck, B., Barrier, E., Biju-Duval, B., Brunet, M.-F., Cadet, J.P., Crasquin, S., Sandulescu, M., 2000. Peri-Tethys Palaeogeographical Atlas. Gauthier Villars.
Evans, D.A.D., 2003. True polar wander and supercontinents. Tectonophysics 362, 303–320.
Evans, I., Hall, S.A., Carman, M.F., Senalp, M., Coskun, S., 1982. A paleomagnetic study of the Bilecik Limestone (Jurassic), northwestern Anatolia. Earth and Planetary Science Letters 61, 199–208.
Fisher, D.A., 1953. Dispersion on a sphere. Proceedings of the Royal Society of London A 217, 295–305.
Gold, T., 1955. Instability of the Earth's axis of rotation. Nature 175, 526–529.
Goldreich, P., Toomre, A., 1969. Some remarks on polar wandering. Journal of Geophysical Research 74 (10), 2555–2567.
Gong, Z., Langereis, C.G., Mullender, T.A.T., 2008. The rotation of Iberia during the Aptian and the opening of the Bay of Biscay. Earth and Planetary Science Letters 273 (1–2), 80–93.
Görür, N., 1988. Timing of opening of the Black Sea basin. Tectonophysics 147 (3–4), 247–262.
Görür, N., 1997. Cretaceous syn- to postrift sedimentation on the southern continental margin of the Western Black Sea Basin. In: Robinson, A.G. (Ed.), Regional and Petroleum Geology of the Black Sea and Surrounding Region, 68. AAPG Memoir, pp. 227–240.
Gutierrez-Alonso, G., Fernandez-Suarez, J., Weil, A.B., Murphy, J.B., Nance, R.D., Corfu, F., Johnston, S.T., 2008. Self-subduction of the Pangaean global plate. Nature Geosciences 1, 549–553.
Heslop, D., McIntosh, G., Dekkers, M.J., 2004. Using time- and temperature-dependent Preisach models to investigate the limitations of modelling isothermal remanent magnetization acquisition curves with cumulative log Gaussian functions. Geophysical Journal International 157, 55–63.
Kirschvink, J.L., 1980. The least-square line and plane and the analysis of paleomagnetic data. Geophysical journal of the Royal Astronomical Society 62, 699–718.
Kruiver, P.P., Dekkers, M.J., Heslop, D., 2001. Quantification of magnetic coercivity components by the analysis of acquisition curves of isothermal remanent magnetisation. Earth and Planetary Science Letters 189, 269–276.
McFadden, P.L., 1998. The fold test as an analytical tool. Geophysical Journal International 135, 329–338.
McFadden, P.L., McElhinny, L.W., 1988. The combined analysis of remagnetization circles and direct observations in palaeomagnetism. Earth and Planetary Science Letters 87, 161–172.
McFadden, P.L., McElhinny, M.W., 1990. Classification of the reversal test in palaeomagnetism. Geophysical Journal International 103, 725–729.
Meijers, M. J. M., Kaymakcı, N., van Hinsbergen, D. J. J., Langereis, C. G., Stephenson, R. A., Hippolyte, J.-C., in press. Late Cretaceous to Paleocene oroclinal bending in the central Pontides (Turkey), Tectonics, doi:10.1029/2009TC002620.
Mileyev, V.S., Baraboshkin, E.Y., Nikitin, M.Y., Rozanov, S.B., Shalimov, I.V., 1996. Evidence that the Upper Jurassic deposits of the Crimean Mountains are allochtons, transactions (Doklady) of the Russian Academy of Sciences. Earth Science Sections 342 (4), 121–124.
The tectonic structure and evolution of the Mountain Crimea. Geological study of Crimea. In: Mileyev, V.S., Rozanov, S.B., Baraboshkin, E.Y., Shalimov, I.V. (Eds.), Geological Faculty MSU Publishers, Moscow (In Russian).
Moix, P., Beccaletto, L., Kozur, H.W., Hochard, C., Rosselet, F., Stampfli, G.M., 2008. A new classification of the Turkish terranes and sutures and its implications for the paleotectonic history of the region. Tectonophysics 451, 7–39.
Mullender, T.A.T., van Velzen, A.J., Dekkers, M.J., 1993. Continuous drift correction and separate identification of ferromagnetic and paramagnetic contributions in thermomagnetic runs. Geophysical Journal International 114, 663–672.
Müller, R.D., Royer, J.-Y., Lawver, L.A., 1993. Revised plate motions relative to the hotspots from combined Atlantic and Indian Ocean hotspot tracks. Geology 21 (3), 275–278.
Muttoni, G., Erba, E., Kent, D.V., Bachtadse, V., 2005. Mesozoic Alpine facies deposition as a result of past latitudinal plate motion. Nature 434 (7029), 59–63.
Nikishin, A.M., Ziegler, P.A., Panov, D.I., Nazarevich, B.P., Brunet, M.-F., Stephenson, R.A., Bolotov, S.N., Korotaev, M.V., Tikhomirov, P.L., 2001. Mesozoic and Cenozoic evolution of the Scythian Platform–Black Sea–Caucasus domain. In: Ziegler, P.A., Cavazza, W., Robertson, A.H.F., Crasquin-Soleau, S. (Eds.), Peri-Tethys Memoir 6: Peri-Tethyan Rift/Wrench Basins and Passive Margins, 186. Mémoires Muséum national d'Histoire naturelle, Paris, pp. 295–346.
Ogg, J.G., 2004. The Jurassic Period. In: Gradstein, F.M., Ogg, J.G., Smith, A.G. (Eds.), A Geologic Time Scale 2004. Cambridge University Press, Cambridge, pp. 307–343.
Ogg, J.G., Agterberg, F.P., Gradstein, F.M., 2004. The Cretaceous Period. In: Gradstein, F. M., Ogg, J.G., Smith, A.G. (Eds.), A Geologic Time Scale 2004. Cambridge University Press, Cambridge, pp. 344–383.
Okay, A.I., 1989. Tectonic units and sutures in the Pontides, northern Turkey. In: Şengör, A.M.C. (Ed.), NATO Advanced ASI Series. Kluwer Academic Publications, pp. 109–116.
Okay, A.I., Siyako, M., Burkan, K.A., 1991. Geology and tectonic evolution of the Biga peninsula, northwest Turkey. Bulletin of the Technical University of Istanbul 44, 191–256.
Okay, A.I., Şengör, A.M.C., Görür, N., 1994. Kinematic history of the opening of the Black Sea and its effect on the surrounding regions. Geology 22, 267–270.
Okay, A.I., Bozkurt, E., Satır, M., Yiğitbaş, E., Crowley, Q.G., Shang, C.K., 2008. Defining the southern margin of Avalonia in the Pontides: geochronological data from the Late Proterozoic and Ordovician granitoids from NW Turkey. Tectonophysics 461 (1–4), 252–264.
O'Neill, C., Muller, D., Steinberger, B., 2005. On the uncertainties in hot spot reconstructions and the significance of moving hot spot reference frames. Geochemistry, Geophysics, Geosystems 6 (4), Q04003. doi:10.1029/2004GC000784.
Orbay, N., Bayburdi, A., 1979. Palaeomagnetism of dykes and tuffs from the Mesudiye region and rotation of Turkey. Geophysical journal of the Royal Astronomical Society 59, 437–444.
Pechersky, D.M., Safonov, V.A., 1993. Paleomagnetic data and palinspastic reconstruction of the Middle Jurassic to Early Cretaceous position of the Crimean mountains. Geotectonics 27, 89–97.
Pechersky et al., D. M., 1993. Paleomagnetic directions and paleomagnetic pole positions: Data for the former USSR, VNIGRI Institute, St.Petersburg, Russia (unpublished), 8.
Prevot, M., Mattern, E., Camps, P., Daignieres, M., 2000. Evidence for a 20° tilting of the Earth's rotation axis 110 million years ago. Earth and Planetary Science Letters 179, 517–528.
Ricou, L.-E., Burg, J.-P., Godfriaux, I., Ivanov, Z., 1998. Rhodope and Vardar: the metamorphic and the olistostrome paired belts related to the Cretaceous subduction under Europe. Geodinamica Acta 11 (6), 285–309.
Robertson, A.H.F., Dixon, J.E., 1984. Introduction: aspects of the geological evolution of the Eastern Mediterranean. In: Dixon, J.E., Robertson, A.H.F. (Eds.), The Geological Evolution of the Eastern Mediterranean, London, 17. Geological Society Special Publications, pp. 1–74.
Robertson, A.H.F., Üstaömer, T., 2004. Tectonic evolution of the Intra-Pontide suture zone in the Armutlu Peninsula, NW Turkey. Tectonophysics 381, 175–209.
Robinson, A.G., Banks, C.J., Rutherford, M.M., Hirst, J.P.P., 1995. Stratigraphic and structural development of the Eastern Pontides, Turkey. Journal of the Geological Society 152, 861–872.

Rusakov, O.M., 1971. Paleomagnetic Directions and Pole Positions: Data for the USSR — Issue 1. Soviet Geophysical Committee: World Data Center-B, Moscow.
Saintot, A., Angelier, J., Chorowicz, J., 1999. Mechanical significance of structural patterns identified by remote sensing studies: a multiscale analysis of tectonic structures in Crimea. Tectonophysics 313 (1–2), 187–218.
Saintot, A., Brunet, M.-F., Yakovlev, F., Sebrier, M., Erschov, A., Chalot-Prat, F., McCann, T., Polino, R., Stephenson, R.A., 2006a. The Mesozoic–Cenozoic Tectonic Evolution of the Greater Caucasus. European Lithosphere Dynamics. Geological Society London, London.
Saintot, A., Stephenson, R., Stovba, S., Brunet, M.-F., Yegorova, T., Starostenko, V., 2006b. The evolution of the southern margin of eastern Europe (Eastern European and Scythian platforms) from the latest Precambrian–Early Palaeozoic to the Early Cretaceous. In: Gee, D., S.R.A. (Eds.), European Lithosphere Dynamics, 32. The Geological Society of London, London, pp. 481–505.
Sarıbudak, M., 1989. New results and a palaeomagnetic overview of the Pontides in northern Turkey. Geophysical Journal International 99, 521–531.
Satolli, S., Besse, J., Speranza, F., Calamita, F., 2007. The 125–150 Ma high-resolution Apparent Polar Wander Path for Adria from magnetostratigrahic sections in Umbria–Marche (Northern Apennines, Italy): timing and duration of the global Jurassic–Cretaceous hairpin turn. Earth and Planetary Science Letters 257, 329–342.
Satolli, S., Besse, J., Calamita, F., 2008. Paleomagnetism of Aptian–Albian sections from the Northern Apennines (Italy): implications for the 150–100 Ma apparent polar wander of Adria and Africa. Earth and Planetary Science Letters 276, 115–128.
Schmid, S.M., Bernoulli, D., Fügenschuh, B., Matenco, L., Schefer, S., Schuster, R., Tischler, M., Ustaszewski, K., 2008. The Alpine–Carpathian–Dinaridic orogenic system: correlation and evolution of tectonic units. Swiss Journal of Geosciences 101, 139–183.
Şengör, A.M.C., Yilmaz, Y., 1981. Tethyan evolution of Turkey: a plate tectonic approach. Tectonophysics 75 (3–4), 181–241.
Şengör, A.M.C., Yilmaz, Y., Ketin, I., 1980. Remnants of a pre-Late Jurassic ocean in northern Turkey: fragments of the Permian–Triassic Paleo-Tethys? Geological Society of America Bulletin 91 (10), 599–609.
Shillington, D.J., White, N., Minshull, T.A., Edwards, G.R.H., Jones, S.M., Edwards, R.A., Scott, C.L., 2008. Cenozoic evolution of the eastern Black Sea: a test of depth-dependent stretching models. Earth and Planetary Science Letters 265, 360–378.
Shipunov, S.V., 1997. Synfolding magnetization: detection, testing and geological applications. Geophysical Journal International 130 (2), 405–410.
Smethurst, M. 2009. Global Paleomagnetic Database, Version 4.6, February 2005, IAGA.
Stampfli, G.M., Borel, G.D., 2002. A plate tectonic model for the Paleozoic and Mesozoic constrained by dynamic plate boundaries and restored synthetic oceanic isochrons. Earth and Planetary Science Letters 196 (1–2), 17–33.
Stampfli, G.M., Borel, G.D., 2004. The TRANSMED transects in space and time: constraints on the paleotectonic evolution of the Mediterranean domain. In: Cavazza, W., Roure, F., Spakman, W., Stampfli, G.M., Ziegler, P. (Eds.), The TRANSMED Atlas: The Mediterranean Region from Crust to Mantle. Springer Verlag, Berlin, pp. 53–76.
Starostenko, V., Buryanov, V., Makarenko, I., Rusakova, O., Stephenson, R., Nikishin, A., Georgiev, G., Gerasimov, M., Dimitriu, R., Legostaeva, O., Pchelarov, V., Sava, C., 2004. Topography of the crust–mantle boundary beneath the Black Sea Basin. Tectonophysics 381, 211–233.
Steinberger, B., O'Connell, R.J., 1998. Advection of plumes in mantle flow; implications on hotspot motion, mantle viscosity and plume distribution. Geophysical Journal International 132, 412–434.
Steinberger, B., Torsvik, T.H., 2008. Absolute plate motions and true polar wander in the absence of hotspot tracks. Nature 452, 620–623.
Steinberger, B., Torsvik, T. H., in revision. Explanation for the present and past locations of the poles, Geochemistry, Geophysics, Geosystems.
Stephenson, R.A., Mart, Y., Okay, A., Robertson, A.H.F., Saintot, A., Stovba, S., Kriachtchevskaia, O., 2004. Transect VIII: Eastern European Craton to Arabian Craton (Red Star to Red Sea). In: Cavazza, W., Roure, F.M., Spakman, W., Stampfli, G.M., Ziegler, P.A. (Eds.), The TRANSMED Atlas — The Mediterranean region from crust to mantle. Springer Verlag, Berlin Heidelberg.
Tauxe, L., Kent, D.V., 2004. A simplified statistical model for the geomagnetic field and the detection of shallow bias in paleomagnetic inclinations: was the ancient magnetic field dipolar? In: Channell, J.E.T., Kent, D.V., Lowrie, W., Meert, J.G. (Eds.), Timescales of the Paleomagnetic Field, 145. AGU Geophysical Monograph, pp. 101–115.
Tauxe, L., Watson, G.S., 1994. The foldtest: an eigen analysis approach. Earth and Planetary Science Letters 122, 331–341.
Tekeli, O., 1981. Subduction complex of pre-Jurassic age, northern Anatolia, Turkey. Geology 9, 68–72.
Torsvik, T.H., Muller, R.D., Van der Voo, R., Steinberger, B., Gaina, C., 2008. Global plate motion frames: toward a unified model. Reviews of Geophysics 46. doi:10.1029/2007RG000227 RG3004.
Tüysüz, O., 1999. Geology of the Cretaceous sedimentary basins of the Western Pontides. Geological Journal 34, 75–93.
Van der Voo, R., 1968. Jurassic, Cretaceous and Eocene pole positions from northeastern Turkey. Tectonophysics 6 (3), 251–269.
Van der Voo, R., 1990. The reliability of paleomagnetic data. Tectonophysics 184, 1–9.
van Hinsbergen, D.J.J., Hafkenscheid, E., Spakman, W., Meulenkamp, J.E., Wortel, R., 2005. Nappe stacking resulting from subduction of oceanic and continental lithosphere below Greece. Geology 33 (4), 325–328.
Van Velzen, A.J., Zijderveld, J.D.A., 1995. Effects of weathering on single domain magnetite in early Pliocene marls. Geophysical Journal International 121, 267–278.
Vandamme, D., 1994. A new method to determine paleosecular variation. Physics of the Earth and Planetary Interiors 85, 131–142.
Waldhör, M., Appel, E., 2006. Intersections of remanence small circles: new tools to improve data processing and interpretation in palaeomagnetism. Geophysical Journal International 166 (1), 33–45.
Watson, G., 1983. Large sample theory of the Langevin distributions. Journal of Statistical Planning and Inference 8, 245–256.
Yılmaz, C., Kandemir, R., 2006. Sedimentary records of the extensional tectonic regime with temporal cessation: Gumushane Mesozoic Basin (NE Turkey). Geologica Carpathica 57 (1), 3–13.
Yılmaz, C., Şen, C., Özgür, A.S., 2003. Sedimentological, paleontological and volcanic records of the earliest volcanic activity in the Eastern Pontide Cretaceous volcanic arc (NE Turkey). Geologica Carpathica 54 (6), 377–384.
Zijderveld, J.D.A., 1967. A. C. demagnetization of rocks: analysis of results. In: Collinson, D.W., Creer, K.M., Runcorn, S.K. (Eds.), Methods in Palaeomagnetism. Elsevier, Amsterdam, New York, pp. 254–286.
Zonenshain, L.P., Le Pichon, X., 1986. Deep basins of the Black Sea and Caspian Sea as remnants of Mesozoic back-arc basins. Tectonophysics 123, 181–211.